Publications of the Astronomical Society of the Pacific
**109:** 173–207, 1997 February

# Atmospheric Intensity Scintillation of Stars. I. Statistical Distributions and Temporal Properties

DAINIS DRAVINS, LENNART LINDEGREN, AND EVA MEZEY

Lund Observatory, Box 43, S-22100 Lund, Sweden
Electronic mail: dainis@astro.lu.se, lennart@astro.lu.se, evam@astro.lu.se

ANDREW T. YOUNG

Department of Astronomy, San Diego State University, San Diego, California 92182-1221
Electronic mail: aty@mintaka.sdsu.edu

*Received 1996 June 20; accepted 1996 November 12*

**ABSTRACT.** Stellar intensity scintillation in the optical was extensively studied at the astronomical observatory on La Palma (Canary Islands). Photon-counting detectors and digital signal processors recorded temporal auto- and cross-correlation functions, power spectra, and probability distributions. This first paper of a series treats the temporal properties of scintillation, ranging from microseconds to seasons of year. Previous studies, and the mechanisms producing scintillation are reviewed. Atmospheric turbulence causes 'flying shadows' on the ground, and intensity fluctuations occur both because this pattern is carried by winds, and is intrinsically changing. On very short time scales, a break in the correlation functions around 300 $\mu$s may be a signature of an inner scale ($\simeq$3 mm in the shadow pattern at wind speeds of 10 m s$^{-1}$). On millisecond time scales, the autocorrelation halfwidth decreases for smaller telescope apertures until $\simeq$5 cm, when the 'flying shadows' become resolved. During any night, time scales and amplitudes evolve on scales of tens of minutes. In good summer conditions, the flying-shadow patterns are sufficiently regular and long-lived to show anti-correlation dips in autocorrelation functions, which in winter are smeared out by apparent wind shear. Recordings of intensity variance together with stellar speckle images suggest some correlation between good (angular) seeing and large scintillation. Near zenith, the temporal statistics (with up to twelfth-order moments measured) is best fitted by a Beta distribution of the second kind ($F$-distribution), although it is well approximated by log-normal functions, evolving with time.

## TABLE OF CONTENTS

## 1. INTRODUCTION

The Earth's turbulent atmosphere causes stars to 'twinkle,' i.e., to undergo rapid fluctuations in their measured intensity as seen on the ground. In this work, we present extensive studies of such intensity scintillation, measured at the astronomical observatory on La Palma (Canary Islands).

A broad literature exists about how the atmosphere influences stellar images. However, most studies concern the more basic *image structure and motion* ('seeing') rather than fluctuations in *intensity* ('scintillation'). Already simple effects in geometrical optics lead to angular displacements, while only (differential) effects of higher order also cause the intensity to be modulated. Angular displacements are caused by the *tilt* of a wavefront, while intensity scintillation originates from wavefront *curvature* (refractive-index variations in air do not cause dissipation of optical energy; fluctuations in irradiance require focusing by turbulent elements).

The number of more complete reviews of stellar scintillation is rather limited; relevant ones include Jakeman et al. (1978), Lee (1969), Reiger (1963), Roddier (1981), and Young (1971a), while a historical overview with references going back to Aristotle is included in Nettelblad (1953).

Efforts by many theoreticians have led to an essentially complete theory of wave propagation in at least some types of weakly inhomogeneous random media (e.g., those whose refractivity fields can be described by power-law spectra; Tatarski 1961; Uscinski 1977). However, the theories do not describe more 'ill-behaved' or 'semi-random' phenomena which often are the realities confronting any observational astronomer. These include evolving thin-layer structures in the upper atmosphere, temperature inversion conditions, and approaching weather fronts.

Recent efforts by observers have often been directed at the verification of functional dependences predicted by some particular theory, rather than systematic analyses of actual atmospheric behavior. Also, most studies are from 'ordinary' sites rather than mountaintop observatories. More detailed studies have been made in exploiting scintillation for probing properties of the upper atmosphere, as well as in laser light propagation over horizontal paths, exploring (and exceeding) the limits to theories for weakly inhomogeneous media.

The purpose of the present work is not to introduce any new physical models of scintillation as such. The accuracy limits in *post-facto* modeling, nowcasting (i.e., from real-time micro-meteorological measurements), or forecasting of atmospheric scintillation are not set by incomplete knowledge of the laws of optics, but by the complex and sometimes rapidly changing weather conditions. Rather, an aim of the present work is to better understand the actual statistical properties of scintillation at premier observatory sites such as La Palma. A fuller mapping of such phenomena is relevant also for the design of second-order adaptive optics, correcting not only phase errors in the wavefront, but also its amplitude, thus eliminating scintillation effects.

Another main motivation behind this project comes from the need to better understand high-speed phenomena in scintillation, in order to detect very rapid intrinsic fluctuations in astronomical objects. Such may arise from instabilities in

mass flows around compact objects—white dwarfs, neutron stars, or presumed black holes—on expected time scales of milli- or even microseconds (Dravins 1994). For a ground-based telescope, such fluctuations will be superposed on the atmospheric ones, and an accurate measurement, calibration, understanding, and segregation of these must precede any astrophysical conclusions.

The twinkling of stars has of course been studied since very long ago. Many studies in the past, however, were based upon limited measurements (perhaps hours), using modest optical apertures (perhaps centimeters), and often made at sites with not the best atmospheric conditions. What is different in the present work is the extensive sets of observations (24 full observing nights at a premier observatory site), using photon-counting detectors with on-line digital signal processing, and also the use of larger telescope apertures. This permits the study of *very* rapid fluctuations even in very small apertures, and an extrapolation to the very largest telescopes. As presented below, these data indeed reveal many new details in scintillation properties, which in the past were hidden in noise.

This project is documented in a series of papers as follows: the present Paper I, *Statistical Distributions and Temporal Properties* covers topics such as the proximity to log-normal intensity distributions, the temporal structure seen in autocorrelations and power spectra, and how these functions evolve over time of night and time of year. Paper II, *Dependence on Optical Wavelength* (Dravins et al. 1997a), deals with differences in amplitudes and time scales, and with delays in cross correlation between scintillation in different colors. The final Paper III, *Effects for Different Telescope Apertures* (Dravins et al. 1997b) evaluates how scintillation manifests itself in different types of telescope (e.g., varying diameter and central obscuration). Scintillation properties are predicted for very large telescopes of the 8-meter class, and techniques outlined for reducing effects of scintillation (apodized apertures, special site selection), and even eliminating them through second-order adaptive optics (as required also for critical imaging applications, such as ground-based studies of planets around other stars).

## 2. THE OBSERVATORY, INSTRUMENTATION, AND MEASUREMENTS

### 2.1 The La Palma Site

For the present program, a 60-cm telescope of The Royal Swedish Academy of Sciences was used. This is located at 2,360 m altitude in the Spanish-International observatory near the summit of Roque de los Muchachos on the island of La Palma, Canary Islands. La Palma is one of the world's best sites for optical astronomy: its properties, as well as (angular) seeing data, together with macro- and micrometeorological statistics obtained from the ground and in the air, are described by Ardeberg (1984), Coulman et al. (1995), de Vos (1993), Dunlop et al. (1989), Muñoz-Tuñón and Fuentes (1990), Nightingale and Buscher (1991), Redfern (1991), Rosa and Fuensalida (1990), and Vernin and Muñoz-Tuñón (1992, 1994). Data collected from balloon soundings show that in the generally stable, nighttime atmosphere, the vertical profile of the microscale temperature-structure function (hence the refractive-index function) consists of a comparatively low-level background and a number of 'peaks', i.e., thin 'seeing' layers or laminae, where the temperature gradient is particularly steep, and which affect the optical propagation. Because of seasonal differences in the weather patterns (summer offering the most stable conditions), observations in this project were made during both winter and summer.

### 2.2 The Telescope

The telescope used is a Cassegrain reflector with optical diameter ∅60 cm, and a secondary mirror mount (∅17 cm), held by four spider vanes. Most measurements were made through apertures other than the full one (i.e., smaller diameter, double, or apodized). For this purpose, the telescope was equipped with a rotatable aperture mask. The largest free circular aperture that is not affected by the secondary mirror has diameter 22 cm, and such an aperture was used in the winter campaign. Other aperture diameters then were prepared in steps of a factor 0.4: the next were ∅9 and 3.6 cm. In the summer campaign, circular apertures in steps of a factor 0.5 were used: ∅20, 10, 5, 2.5, and 1.2 cm. These apertures were cut out in an opaque mask, mounted in front of the telescope tube, and with a shutter covering all openings except the one in current use. A switch to any aperture in this mask could be done remotely within a few seconds of time, by rotating the shutter. A change to the full telescope opening, however, required a physical removal of the aperture mask, an operation of some 5–10 minutes.

### 2.3 Instrumentation

The measuring instrument used, QVANTOS (Quantum-Optical Spectrometer; Dravins et al. 1994), was constructed as part of a program in observational high-speed astrophysics. Its Mark I version used here is basically a computer-controlled high-speed photometer with rapid photomultipliers, and fast real-time digital signal processors.

The optical assembly and the detectors were mounted at the Cassegrain focus, with signal cables going to signal processors and data displays on the observing floor. A beam-splitter first divides the light from the telescope into two paths. One goes to a TV-camera for guiding, and the other to the detectors. In front of these, filters may be inserted. Normal photometer optics were employed, e.g., a Fabry lens imaged the telescope aperture onto the central area (∅2.5 mm) of the photocathode. Much of the time only one (always the same) of the photomultipliers was used, but in cross-correlation measurements two were used together, following another beamsplitter. A retroreflector was used to adjust the light paths, and to find the position of the photomultiplier aperture on the TV-monitor.

The detectors are two nominally identical, EMI 9863B/100 photon-counting photomultipliers (PMT), with S-20 spectral response (maximum sensitivity in blue, but extending also to the red). The time response of the system is very fast throughout: the pulse rise time is typically 2.5 ns, the full width at half-maximum (FWHM) ≃4 ns, amplitude-

discriminator electronics rise time <3 ns, etc. This stream of photon-count pulses is analyzed in a real-time signal processor (basically a Malvern Instruments K7026 digital correlator), with a cycle time of 20 ns. This unit is, in turn, controlled by a desktop computer for instrument control, data storage, and preliminary data analysis.

Interference filters centered at wavelengths of 400, 500, 550, 600, and 700 nm, with FWHM $\Delta\lambda \simeq 70$ nm were used to select wavelength ranges. Their transmission profiles are rather symmetric, although a few filters show faint (few %) tails out toward longer wavelengths. This is of little significance since the sources observed were 'white' stars, and the PMT sensitivity drops rapidly toward longer wavelengths. A few narrow-band filters were used in near ultraviolet: $\lambda$ 365 nm, $\Delta\lambda \simeq 10$ nm, as well as for a narrower passband than usual: $\lambda$ 540 nm, $\Delta\lambda \simeq 10$ nm. Also, measurements in 'white light', i.e., without any filter, were made. In this case, the color extent ($\Delta\lambda \simeq 300$ nm) is set by a combination of the typically white starlight, and the PMT's color response, resulting in an essentially flat response curve from the violet to $\lambda \simeq 600$ nm, and then dropping rapidly for longer wavelengths. Various neutral density filters were used to adjust the count rate to a suitable level. Different filters could be placed either at each of the two PMT's, or made common to both detectors, placed in front of their beamsplitter.

The system was programmed to give either (a) the probability density function (PDF), i.e., a histogram for the number of time intervals (of preselected duration) during which there were recorded exactly 0,1,2,3,...,63 photon counts (since events with $\geqslant 64$ counts were not recorded, the sample times were chosen so that the maximum count numbers were well below 64); (b) 64-point temporal autocorrelation (ACO) function in time (with a preselected time-lag interval), or (c) an analogous cross-correlation function (CCO) between the counts from two different photomultipliers. The sample-time duration was set in software between 20 ns and 10 s. Typically, values between 100 ns and 100 ms were used, changed in steps of a factor 10.

To be suitable for measuring statistical functions of variability, our detectors were selected among others of nominally identical manufacture, not only for maximum sensitivity and low dark count but, in particular, for exceptionally low afterpulsing (e.g., the measured afterpulsing in that PMT mostly used was only $\simeq 1\%$ of that in another nominally identical tube). Further, most of these effects occur on time scales much shorter ($\simeq 50$ ns) than those typical for the atmosphere. Even so, for our most accurate recordings, cross-correlation functions between two different (but nominally identical) detectors were measured to further eliminate effects of correlated noise (see the Appendix below).

The output after each measurement (typically of 100-s integration), thus consists of a statistical function with 64 points, plus some information on the total number of counts, etc. These data are then output to the computer together with the observation log, forming the basis for our following discussion. A schematic diagram of the instrumentation is in Fig. 1.

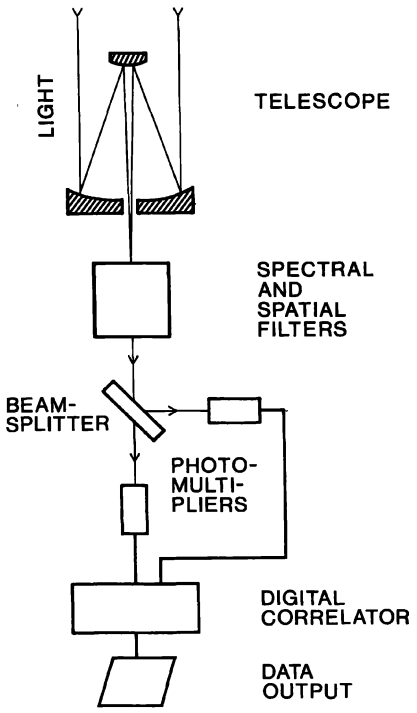


FIG. 1—Schematic layout of the QVANTOS Mark I instrument, used for studying stellar scintillation on La Palma. This is essentially a very fast stellar photometer, whose digital signal processor is capable of handling large volumes of data in real time. When required, effects of correlated detector noise can be minimized through the use of two detectors, whose output pulse trains are cross correlated.

### 2.4 Observations

As targets, ordinary single stars were selected (except when specifically studying binaries). None of these is expected to have any measurable intrinsic variation on the time scales studied, so all variability detected can be ascribed to the atmosphere. Different stars were selected depending on the aim of any particular measurement series. For example, to study changes over a night, Polaris was often used. Thanks to its position close to the celestial pole, it remains at an almost constant position in the sky, eliminating dependences on varying airmass at different zenith angles, or changes with azimuth.

Otherwise, bright stars some 30° apart in the sky were selected in order to have targets at different zenith-horizon distances throughout the nights. Stars of a generally white color were chosen, enabling efficient measurements in the violet as well as in the red spectral regions. The brightness of the stars permitted high time-resolution measurements also for small telescope apertures and narrow-band filters. When looking for scintillation effects from closely adjacent stars, binaries with equally bright components were looked for.

The target star was acquired with the telescope and centered within the photometer diaphragm. Its position was continuously monitored on a TV screen, fed by an image-intensifying speckle camera. To avoid possible disturbances to the electronics, no guiding corrections were ever applied to the telescope during actual observations. During the win-

ter campaign, only stars in such sky positions were observed, where the telescope's tracking system performed well enough to keep the star centered without any adjustments during integration. During the summer campaign, an ultrafine guiding system inside the instrument was used to keep the star's optical image centered (by moving crossed prisms), fed by low-voltage motors only, not connected to any other electronics.

Two extensive observing campaigns were carried out, one in winter (November/December), and one in summer (July/August). Not counting nights for instrument tests and some lost to poor weather, about 11 effective ('full') nights were utilized for observations during the winter, and 13 full nights during summer. The number of scintillation functions recorded exceeded 1,000 in the winter campaign, and 1,500 in the summer one.

## 3. PREVIOUS SCINTILLATION STUDIES

In this chapter we give a general overview of previous main results from studies of stellar scintillation, putting our work in perspective. In the literature, there unfortunately exists no complete and up-to-date review on the topic. The most recent one of some breadth is by Jakeman et al. (1978). While several reviews in optical physics are devoted to wave propagation in idealized random media, they are not always relevant for the actual conditions above astronomical observatories. Comments on previous results for more specific topics will also be made later in the respective sections.

### 3.1 Basic Properties of Scintillation

The 'amount' of scintillation can be measured by the variance $\sigma_I^2$ of the relative fluctuations in intensity $I$, $\sigma_I$ being the root-mean-square value of $(I-\langle I\rangle)/\langle I\rangle = \Delta I/\langle I\rangle$, where $\langle\ \rangle$ denotes time average. In the literature, $\sigma_I^2$ is often called the "scintillation index" (although that expression has been used also for the rms modulation of $I$ itself). To avoid ambiguity, for $\sigma_I^2$ we will use the term 'intensity variance.' The 'rate' of scintillation can be measured by the width of the temporal correlation function or, equivalently, by its Fourier transform, the power spectrum. Especially in older literature, the "frequency" of scintillation expresses how often the fluctuating intensity crosses its average value. The values for intensity variance $\sigma_I^2$ in our work refer to the variance of the *linear* quantity. In some publications, the variance is instead given for the *logarithm* of intensity, the relation being $\sigma_I^2 = [\exp(\sigma^2_{\ln(I)}) - 1]$. For small scintillation amplitudes, the difference is negligible.

A refractive-index undulation in the atmosphere acts as a lens, focusing the starlight. The illumination of a screen (=pupil plane) at some distance from such a lens varies from place to place because alternate sections of the lens are converging and diverging. Scintillation involves a geometrical "lever-arm" effect, since the wave front wiggles must be sufficiently distant to produce brightness changes. Scintillation is normally dominated by turbulence at high altitudes (many kilometers), while [angular] seeing often has significant components originating close to the telescope.

When the turbulence causing the refractive fluctuations is at a great distance from the telescope, the irradiance becomes variable in both space and time. This intensity modulation can be observed in short-exposure images of a telescope mirror illuminated by a bright star, as a system of rapidly moving 'shadows.' With the unaided eye, such 'flying shadows' can be glimpsed during the moments before and after a total solar eclipse, when an uneclipsed solar crescent acts as the light source. Then the 'shadows' appear as elongated 'bands' because of the anisotropic brightness distribution of the solar crescent. Their motions are determined by wind components at various contributing altitudes. However, in contrast to solar eclipse phenomena, shadow patterns from stars are statistically isotropic. Scintillation may be studied either by measuring the fluctuations in image intensity, or by measuring the shadow pattern directly.

The intensity of the telescopic image depends upon the sample of the shadow pattern selected by the telescope at any instant. Temporal variations occur for two main reasons. Firstly, the shadow pattern moves across the detector as the region of atmosphere producing the pattern is carried by the wind. Most modeling indeed assumes that this pattern can be regarded as frozen in the atmosphere [Taylor's approximation], merely swept by winds across the telescope aperture. However, fluctuations also occur when the structure of the shadow pattern varies due to changes in the turbulence, or due to the relative motion of different regions of the atmosphere. Detailed studies of the spatio-temporal properties of scintillation for single and binary stars can be used to deduce quite detailed information about the often layered structure in the upper atmosphere.

In order to 'fully' resolve the atmospheric effects, it is necessary to limit the size of the telescope pupil, the spectral bandwidth of the detector, and the sample time of the processing equipment. Aperture averaging will reduce the variance unless the telescope aperture is significantly smaller than the smallest feature size in the shadow pattern. Thus a measure of the variance as a function of aperture size gives an estimate of these feature sizes.

Different extents of the sampling aperture, and of the temporal integration, preferentially 'filter' out differently distant turbulence elements. For example, naked-eye twinkling ($\simeq$5 mm aperture, a cutoff for frequencies above $\simeq$15 Hz), arises mostly from turbulence within 1 km of the ground.

### 3.2 Earlier Studies

Scintillation of stars has been studied for a very long time, and the introduction of new techniques at successive epochs has gradually revealed new information. Until the advent of photoelectric photometry, the only way of registering scintillation (besides visual observations) was by photography. Although there were many such studies, not very much of a quantitative nature was achieved. The earliest work that directly bears upon our present project, are the systematic photoelectric measurements in the 1950's. These were made possible by the advent of photomultipliers, oscilloscopes, and other electronics, permitting quantitative studies of the amplitudes and the temporal frequency contents up to $\simeq$1 kHz. Quite extensive studies were made during a number of

years, surveying scintillation dependence on visual seeing, zenith distance, altitude above sea level, size and shape of telescope aperture, differences between stars and planets, changes with season, and between different observatory sites. Detailed studies at this epoch were by Keller et al. (1956), Mikesell (1955), and Protheroe (1955a), with overviews by Briggs (1963), Elsässer (1960), Mikesell et al. (1951); and Protheroe (1961).

Mikesell (1955) found that 'artificial stars' (i.e., small lamps) on high-altitude balloons, showed rather less scintillation than adjacent real ones, demonstrating that scintillation originates in the upper atmosphere. Mikesell (1955) and Protheroe (1955a) could correlate scintillation with the wind-speed at heights between 8–16 km, but not with that at lower levels. Protheroe (1955b, 1964) also found the speed and direction of the 'flying shadows' to correlate reasonably well with upper-air winds. The lifetime of elements in the shadow pattern was found to be on the order of 10 ms.

### 3.3 Understanding Scintillation

Based upon the then improved understanding of atmospheric turbulence, Reiger (1963) derived analytic expressions for the correlation function and power spectra of stellar scintillation. In his atmospheric model with turbulent motion (a Kolmogorov spectrum with a $-11/3$ power law for wave number) and a continuous distribution with height of refractive-index fluctuations, more than 70% of the scintillation amplitude originates in the height range from 7 to 15 km. The theory is a monochromatic one, based entirely on geometrical optics.

Reiger's theory predicts the two-dimensional brightness spectrum in the plane of the telescope aperture. This space variation is converted to a one-dimensional (time) variation by the motion of the shadow pattern across the aperture, which acts as a spatial filter. Since the filter function is the squared Fourier transform (diffraction pattern) of the aperture, the dependence of the scintillation spectrum on the size and form of the aperture is readily understood.

Young (1967) confirmed Reiger's theory of scintillation by additional observations, including such for larger air masses and large telescope apertures. The power of scintillation is nearly independent of wavelength, and is proportional to the cube of the air mass and (at low frequencies) to the $-4/3$ power of the telescope aperture. Nevertheless, the theory by Reiger (1963) is not complete, for it does not include wave (interference) effects, which must modify the spectra at high frequencies and large zenith distances. Young (1969, 1971a) generalized the theory to allow for finite source sizes (planetary scintillation), effects of diffraction, atmospheric dispersion, and seeing.

### 3.4 Recent Studies

More recently, photon-counting detectors and digital signal processors have permitted studies of more subtle phenomena. Following a limited study by Jakeman et al. (1976), Dainty et al. (1982) explored scintillation on Mauna Kea in Hawaii, at 4,200 m altitude. They mainly searched for changes with optical wavelength, but recorded also higher statistical moments in the temporal distribution of irradiance. In another extensive study, Stecklum (1985) made high-speed correlation and statistics measurements, obtaining up to fourth-order moments.

Besides for the study of scintillation *per se*, an astronomical interest is to examine how scintillation affects observations of stars being occulted by, e.g., the Moon (Knoechel and von der Heide 1978), or observations of high-speed phenomena in general (Warner 1988). It can also be applied to study *planetary* atmospheres, from observing the 'twinkling' of stars during planetary occultations. In the ultraviolet, even studies of the *solar* atmosphere could become possible, from occultations of stars by the solar limb.

### 3.5 Scintillation from Space

A few observations exist of stars setting in the Earth's atmosphere, seen from space. This permits the study of high-elevation (20–40 km) atmospheric layers, whose influence on ground-based scintillation is small. The results (e.g., Aleksandrov et al. 1990) show that the temperature inhomogeneities are highly anisotropic also in the stratosphere, being elongated in the direction of the Earth's surface (apparently analogous to the 'sheets' of temperature inhomogeneities seen at lower levels: Dalaudier et al. 1994; Vernin et al. 1979).

The atmosphere is vertically asymmetric, and the problem of observing scintillation of an extraterrestrial source from the ground is *not* equivalent to that of observing scintillation of a terrestrial source from space. Although there are issues in common, we will not discuss them further; for examples of current experiments, see Lightsey (1994).

## 4. CONCEPTS IN SCINTILLATION THEORY

In our interpretation of data, and in predicting scintillation in different types of telescopes, we will use models and their scaling properties. While it should not be expected that this modeling will reproduce all observations down to their last significant digit, it is able to illustrate the functional dependence on several parameters. In this chapter, we review the concepts for such models, and especially point out their various limitations.

Scintillation is caused by refractive-index inhomogeneities in clear air. These variations (some $10^{-6}$) are related primarily to the small changes in temperature (on the order of 0.1–1 K), accompanying turbulent motions in the atmosphere. Although each inhomogeneity may be tiny, light propagates through a large number of them, and the cumulative effect is significant.

Atmospheric turbulence has a random structure, producing random effects on light that passes through it. The three-dimensional turbulence and the two-dimensional wavefront require a statistical description: either by autocorrelation functions, spatial wavenumber spectra, or structure functions (i.e., mean-square differences between two points at different separations). These three descriptions are integral transforms of one another, and so are (for practical purposes) equivalent, although structure functions remain well defined even when some of the other integrals diverge at large scales (in particu-

lar, for nonstationary processes without a well-defined mean; Tatarski 1961). While Tatarski and his followers developed the theory in terms of structure functions, most astronomers use power spectra or correlation functions, and the theory is generally easier to understand in terms of these.

### 4.1 Statistical Descriptions of Turbulence

The nature of turbulence on the scales of importance for astronomical observations is closely described by an isotropic power-law spectrum (or the equivalent autocovariance, or structure function), first derived from dimensional considerations by Obukhov and Kolmogorov half a century ago. The validity of this Kolmogorov (or Obukhov-Kolmogorov) law has since been confirmed for many physical situations (Lumley and Panofsky 1964; Frisch 1995).

However, astronomers were concerned with scintillation long before this law was discovered. One had noted the 'shadow pattern' with typical scales of about 10 cm illuminating the telescope pupil, and worked with the idea that both this pattern and the turbulence producing it could be described by Gaussian patches of about this size. Thus the early astronomical literature on scintillation uses an incorrect assumption about the very nature of the phenomenon, and is rife with talk of Gaussian correlation functions and a single characteristic scale. This, we now know, is completely wrong. Nevertheless, because of inertia (and astronomers' ignorance of the turbulence literature) it persisted well beyond Reiger's (1963) introduction of the correct functional dependence into the stellar-scintillation literature.

The actual structure of turbulence is quite different. Because it is statistically described by a power law, it is self-similar at all scales of interest; no particular length is characteristic of the turbulence. Such a power-law description of turbulence necessarily diverges at either very large or very small scales (the large scales diverge for the Kolmogorov law). Physically, this divergence is to be prevented by a spectrum truncation at some 'outer scale,' where energy is fed into the turbulence. However, the size of this outer scale is quite uncertain, and is also unimportant for scintillation, which is determined by wavefront *curvatures* rather than phase delays.

The Kolmogorov law is supposed to die out at some small 'inner scale' (believed to be on the order of a few mm) at which viscosity begins to damp the random motions, which have been passed on to ever smaller scales by wind shear and vorticity. In most practical measurements, the inner-scale irregularities are hidden because the Fresnel-zone size (typically several cm) filters out smaller features. In fact, it is the Fresnel-zone size that characterizes the features in the shadow pattern. In addition, even features this small are usually hidden by the telescope aperture, which is often much larger.

Thus, although turbulence itself has two characteristic scales (inner and outer), neither of these is very apparent in astronomical observations. In nearly all cases, the characteristic scale that dominates the observations is the size of the telescope aperture itself.

The interval between the inner and outer scales is called the 'inertial subrange,' because the turbulent energy cascades from larger to smaller scales by mixing and tearing motions. Because the randomization of the motions becomes more complete as the mixing progresses, the structure is highly isotropic at scales appreciably smaller than the outer scale (including those important for scintillation). This isotropy provides convenient relations among one-dimensional measurements (such as temperature-structure functions), the three-dimensional structure of the turbulence itself, and the two-dimensional shadow pattern it produces.

### 4.2 Wave Propagation through the Atmosphere

In this large field of research, most [astronomical] efforts have been directed toward understanding the origins of *seeing*, i.e., the spread in *angular* direction and image size. Only a modest number of modern papers have been devoted to astronomical intensity scintillation, although there is a substantial [non-astronomical] literature on, in particular, fluctuations arising in laser beam propagation.

A clear and concise introduction to issues in optical propagation is by Consortini (1991), while more technical ones are by Kravtsov (1992, 1993). Intensity fluctuations for various combinations of wave (plane, spherical) and random-medium properties, were surveyed by Lawrence and Strohbehn (1970). Clifford (1978) reviews the classical theory of wave propagation in turbulent media (including different models for atmospheric turbulence), and Strohbehn (1978) theories oriented towards laser beam propagation. Weak scattering arising in random-phase-screens (i.e., disturbing layers) was discussed by Lee and Harp (1969). A number of monographs exist on wave propagation in random media: Ishimaru (1978); Rytov et al. (1989); Uscinski (1977); as well as the classical ones by Tatarski (1961, 1971).

Mathematical solutions of the equation for the fourth-moment of wave amplitude, predicting scintillation power spectra, are possible for some physical and geometrical situations. For an example of an analytical treatment, see Uscinski (1985) for a medium containing a large number of equally spaced weak phase-modulated screens. For a numerical treatment instead, see Tur (1985) for a two-dimensional isotropic random medium with a Gaussian correlation function.

To reveal the intensity distributions ('flying shadows') resulting after wave propagation through the atmosphere, laboratory experiments can be made (Parry et al. 1977), as well as numerical simulations (Martin and Flatté 1988). Resulting statistical functions of irradiance, such as probability densities or correlation functions, can likewise be computed numerically (Flatté et al. 1994) or, in some cases, analytically (Cook 1991).

### 4.3 Modeling Scintillation

Theories of scintillation often begin with a 'phase-changing screen'—a thin slab of turbulent medium that deforms the smooth incident wavefront. The angular seeing depends on the slopes of the deformed wavefront, while scintillation depends on the *curvature*, because it involves focusing and defocusing. Thus, the seeing depends on the

first derivative of the phase-fluctuation power spectrum, while scintillation depends on the second derivative.

Theories of scintillation have been developed for both wave-optical treatments, and geometrical-optics approximations; using either the spatial power spectrum of the refractive-index fluctuations, or corresponding structure functions (Roddier 1981; Young 1969, 1970a, b).

Consider a plane wave passing through a 'phase screen,' i.e., a thin slab of turbulence. Irregular phase delays cause the emergent wavefront to become wrinkled. Each Fourier component of turbulence in the slab corresponds to a sinusoidal phase grating, from which the wavefront emerges with sinusoidal corrugations of a spatial period $d$. We can analyze this wavefront in terms of its angular components, i.e., in terms of the first- and higher-order spectra diffracted by the grating. For weak turbulence, the corrugations are small, and only the first-order diffracted waves have appreciable amplitudes. These diffracted waves interfere with the zero-order wave to give a sinusoidally modulated diffraction pattern, with the same spatial period $d$. Near the phase screen, the first-order waves are nearly in phase with the zero-order one, so the intensity modulation is small. As we move further away, the phase differences (and hence the modulation in the shadow pattern) increase, reaching maximum when the first-order waves are a half-wave out of phase from the zero order. For a triangle at this distance ($h$) we have $h^2+d^2\simeq(h+\lambda/2)^2$ or $d\simeq\sqrt{\lambda h}$. Thus, diffraction preferentially enhances intensity modulation on spatial scales $\simeq\sqrt{\lambda h}$, which is the Fresnel-zone size $r_F$. In particular, higher frequencies are filtered out by the diffraction. For a star near zenith observed in visual light through high-level turbulence, the expected Fresnel-zone size $r_F$ is on the order of 5–10 cm. These wave-optics effects go away for sufficiently short optical wavelengths. Then we are in the geometrical-optics regime, where the phase screen merely acts like a wavy lens.

For idealized conditions, and the wave-optical description, the intensity variance $\sigma_I^2$ is predicted to vary as:

$$\sigma_I^2 \propto \lambda^{-7/6}\int_0^\infty C_n^2(h)h^{5/6}\mathrm{d}h, \qquad (1)$$

where $\lambda$ is optical wavelength, $C_n^2(h)$ the refractive-index structure coefficient (measuring the optical strength of turbulence), and $h$ is altitude in the atmosphere. The contribution of a turbulence layer to scintillation thus increases with height as the 5/6 power. This integral, weighting $C_n^2(h)$ by the 5/6 power of altitude was found already in the wave-optical treatment by Tatarski (1961). Scintillation decreases with increasing wavelength $\lambda$, and becomes rather small in the infrared.

These results, however, are valid only when irradiance fluctuations are measured through an aperture smaller than their typical scale ($\lesssim$5 cm). In large telescopes, high spatial-frequency components are smoothed out, and a telescope filtering function must be introduced. The geometrical-optics approximation is valid for aperture diameters greater than the diffraction Fresnel-zone size; $D \gg \sqrt{\lambda h}$, i.e., for $\lambda$ 500 nm, and $h=10$ km, $D\gg 7$ cm. In such a case, the amount of scintillation is independent of wavelength and decreases with increasing $D$, according to a $-7/3$ power law:

$$\sigma_I^2 \propto D^{-7/3}\int_0^\infty C_n^2(h)h^2\,\mathrm{d}h. \qquad (2)$$

Such an integral, weighting $C_n^2(h)$ by height squared, was deduced in the geometrical-optics treatment by Reiger (1963). The differences between the wave and geometrical-optics theories are further discussed by Bufton (1973) and Paternò (1976).

The strong altitude-weighting of the contributions implies that the higher (upper troposphere) layers dominate the contributions to scintillation, while effects of low-altitude layers are filtered out. The above expressions are valid for scintillation at the zenith. For moderate zenith angles $Z$, one must replace $h$ by the distance along the line of sight, $h/\cos Z = h\sec Z$. For the wave, and geometrical-optics cases (with $D$ respectively smaller, or greater than the Fresnel-zone size $r_F$), this gives (e.g., Young 1970a; Roddier 1981):

$$\sigma_I^2 \propto \lambda^{-7/6}(\sec Z)^{11/6}\int_0^\infty C_n^2(h)h^{5/6}\,\mathrm{d}h \quad (D<r_F) \qquad (3)$$

and

$$\sigma_I^2 \propto D^{-7/3}(\sec Z)^3\int_0^\infty C_n^2(h)h^2\mathrm{d}h \quad (D\gg r_F). \qquad (4)$$

These seem to be in reasonable agreement with observations up to $Z\simeq 60°$. For greater zenith angles, $\sigma_I^2$ is observed to increase less rapidly, and even to saturate.

### 4.4 Aperture Effects

To compute the expected scintillation in a given telescope, its aperture size and shape must be accounted for. Its spatial-filter function is then multiplied by the two-dimensional power spectrum of the shadow pattern on the ground, and the product is integrated in spatial-frequency dimensions to give the total modulation power. Increasing the telescope aperture diameter preferentially averages out the spatially smallest and temporally fastest fluctuations. The behavior of scintillation spectra with changing telescope aperture has been theoretically investigated by Reiger (1963), Tatarski (1961), and Young (1967, 1969, 1970b), and reviewed by Roddier (1981). For a concise overview of the predictions of scintillation theory, see Stecklum (1985).

### 4.5 Frequency Functions and Correlations

Scintillation in the time domain depends on the wind velocity vector. When observing in zenith, a [horizontal] wind will sweep the shadow pattern across a telescope aperture, at the true windspeed $V_0$. Away from the zenith, the projected speed equals this true speed only at azimuths perpendicular to the wind vector: along the wind azimuth, the apparent speed is reduced by the projection factor $\cos Z$.

It can be shown that spectral power density at low temporal frequencies is inversely proportional to the projected speed $V_\perp$. If the wind is faster, the same total signal variance is spread over a wider band of frequencies. Then the power

per hertz of bandwidth at low frequencies is less, and that at high frequencies is greater, even if the actual turbulence remains the same. Thus, the temporal properties of scintillation change with the azimuth of observation (Young 1969).

The spatial properties of the shadow patterns can be directly measured as the spatial autocovariance function of the intensity (i.e., the spatial autocorrelation pattern of the deviations from the mean). This autocorrelation is the Fourier transform of the one-dimensional spatial power spectrum. Such measurements will be extensively discussed below, starting in Sec. 6.

The theory outlined above allows one to calculate the monochromatic properties of the shadow pattern of a point source, observed with a point detector. The effects of different and finite optical bandwidths will be discussed in Paper II, and aperture filtering, i.e., the scintillation observed behind telescope apertures of different size and shape, in Paper III.

### 4.6 Atmospheric Sources of Scintillation

Finally, we remind the reader that, although there may exist a general understanding as to which laws of optical physics are applicable to scintillation, the small-scale structure of atmospheric inhomogeneities is both very complex and still incompletely understood, and is treated in various idealized approximations.

Actual measurements of the atmospheric microstructure reveal a fairly large number (typically some tens) of very thin ($\simeq$3–20 meters) 'sheets' of temperature increase (by $\simeq$0.2–0.8 K), located at various heights, at least up to the middle stratosphere, but concentrated to the tropopause region between typically 8–15 km altitude. Such data are obtained from fast-response microthermal sensors on high-altitude balloons, from radar echoes, or measuring scintillation of binary stars (Azouit et al. 1980; Barletti et al. 1976, 1977; Bufton 1973; Dalaudier et al. 1994; Rocca et al. 1974; Vernin and Azouit 1983; Vernin and Roddier 1973; Vernin et al. 1979). *In situ* measurements with sensors some distance apart demonstrate that the sheets are neither flat nor horizontal. Vertical distortions appear to be >10 m, and horizontal extensions >100 m. At excellent astronomical observatory sites, the inhomogeneities near the ground are small, although such can be significant at other locations.

By themselves, temperature inversions do not cause scintillation; that requires wind shear to produce turbulence and mixing of air across such inversion layers. Evidence for scintillation connected with thin layers has been sought by observing the changing scintillation of an artificial light source, carried by a rocket to high altitude, and then released on a parachute (Hudson 1965).

The precise modeling of scintillation in such an intermittently inhomogeneous medium is limited by the lack of detailed *in situ* measurements combining air temperature profiles (identifying inversion layers) with temperature difference functions (identifying turbulence). The often used Kolmogorov theory for [three-dimensional] turbulence implies the existence of an inertial subrange over spatial scales where the turbulent elements are at least locally isotropic and homogeneous. However, for developing turbulence, and breaking-wave motion likely to occur in the upper atmosphere, another power law (or another relation) could well apply. For example, the small vertical extent of many *temperature* structures suggests a truncation of the inertial subrange (although the *turbulence* structures might have different scales). In response to such concerns, there have been some efforts to model other types of turbulence distributions, e.g., fractal ones, or with inhomogeneities in the form of triangular wedges in random motion. For a further introduction to relevant issues in atmospheric turbulence and boundary-layer meteorology, see Stull (1988).

Another uncertainty is the assumption, introduced by G. I. Taylor in 1938, of 'frozen-in' turbulence, i.e., the approximation that the atmospheric structures evolve on time scales [much] longer than those required for the wind to blow the shadow pattern past the telescope. It has been argued (Panofsky and Dutton 1984) that this assumption should be valid for frequencies $f$ higher than the vertical gradient of the wind shear (typically some m s$^{-1}$ in a few hundred meters); thus it 'should' hold for $f \gtrsim 0.01$ Hz. Taylor's hypothesis was examined by Caccia et al. (1987) and de Vos (1993) through spatiotemporal cross-correlation studies, estimating lifetimes of certain turbulent eddies. Focusing on one particular atmospheric layer, Taylor's hypothesis appears to be a good approximation for short delays $\lesssim$10 ms, but the shadow pattern becomes decorrelated for time-lags greater than $\simeq$60 ms.

Taylor's hypothesis, however, refers to the *turbulence*, and not necessarily to the shadow pattern. The atmosphere contains many layers with different velocity vectors; each produces its own shadow pattern that could be relatively long-lived; but the *sum* of the patterns remains coherent only if the motions of all turbulent layers are identical. The lifetime of an individual shadow feature is limited by the time it takes the wind shear to move the components a distance equal to their size. As differences in wind velocities between different heights may reach perhaps 10 m s$^{-1}$, and the size of a shadow is a typical Fresnel-zone size ($\simeq$10 cm), one expects the lifetime to be no more than these 10 cm divided by 10 m s$^{-1}$, i.e., about 10 ms (as observed).

Thus, irrespective of whether Taylor's approximation is valid or not, the shadow pattern cannot reasonably remain coherent while crossing any larger aperture: at a windspeed of 10 m s$^{-1}$ it takes one full second for the shadow pattern to fly across a very large telescope.

## 5. SCINTILLATION STATISTICS

In this section, we now examine whether, and how well, the temporal statistics of actual scintillation can be described by various approximations. Elementary small-perturbation theory predicts starlight to be *log-normally* distributed, i.e., the logarithm of the instantaneously measured intensity is expected to obey a Gaussian probability distribution. Although this prediction is widely accepted as correct, there seem to exist but few experimental verifications to any substantial accuracy. For greater zenith distances (where the perturbations may no longer be 'small'), there is actually evidence for deviations from such a law.

### 5.1 Origin of Log-Normal Statistics

The theoretical argument is based on the [Rytov] method of smooth approximation, which implies that the effect of turbulence is to perturb the propagating wave by a large number of independent events (e.g., Tatarskii 1971). The refractive-index variations along a path of propagation modulate the intensity in a multiplicative manner, in the sense that if twice the intensity is transmitted, then twice the variation is observed. The variations included in each subrange then combine multiplicatively so that the atmospheric effect at each point is independent of the initial conditions. Hence such variations modulate the flux in a multiplicative manner, and its logarithm in an additive manner, i.e., the expected variation of log intensity is the sum of many random perturbations induced at various places along the path of propagation. As a consequence of the central-limit theorem, if the number of perturbations [of comparable magnitude] is very large, the variations of log intensity should follow a normal (Gaussian) distribution.

This argument does not involve any assumptions about the correlation or spatial functions of the turbulence, but depends on there being many statistically independent contributions. These may be either spatial frequency components, or independent slabs of turbulence along the line of sight. The central-limit theorem states that the distribution of the sum of independent variates must converge to the normal as the number of comparable variates becomes large, regardless of the distribution of each variate.

However, this argument does assume that there has been a great number of perturbations, for convergence to the log-normal distribution to have occurred. This assumption may be not valid, since the number of [significant] perturbations may be rather finite. Because of the skewness and very long tail of log-normal distributions, the convergence is quite slow (especially in the tails; e.g., Hall 1982; Mitchell 1968), and may not be realized to any degree of accuracy after such a limited number of scatterings.

We note that an incorrect argument was widely used in the days when the erroneous Gaussian correlation function was commonly assumed to apply to both the turbulence and the shadow pattern [e.g., the review (Stock and Keller 1960) in the volume *Telescopes* of the *Stars and Stellar Systems* series that was a standard reference during the 1960s]. This argument involved the false assumption that the patches in the shadow pattern were statistically independent; from which it would follow that their number would increase as the area of the telescope pupil, with the intensity variance decreasing accordingly. If many such independent patches were encompassed by the pupil, the resulting intensity distribution would be Gaussian.

As shown by Young (1970a), this argument is contrary to the observations: it predicts the wrong dependence of the intensity variance on telescope diameter, the wrong dependence on zenith distance, etc. The fallacy in the 'independent patches' argument is that the patches noticed by the eye are not at all statistically independent. As was pointed out by Mertz (1965), turbulence merely redistributes the available energy; conservation of energy requires that a brighter patch be accompanied by darker neighbors. However, Mertz again invoked the 'statistically independent' argument, applying it to the periphery of the pupil instead of its area. Needless to say, this also produced an incorrect diameter dependence.

Because the displacement of rays in the pupil plane is proportional to only the first derivative of the turbulent spectrum, which is a very steeply falling power law, these displacements are largest for the largest spatial components of the turbulence, and are quite tiny for the small-scale features that appear (to the eye) to dominate the shadow pattern. Thus, the small 'patches' a few centimeters across that are so visible to the eye actually contribute negligibly to the net fluctuation averaged over the telescope pupil; this average is dominated by the components comparable in size to the pupil itself, which are the ones capable of moving appreciable flux in or out of the pupil area. Equivalently, we may say that because the turbulence (and hence the shadow pattern) is self-similar at all scales of interest, it is meaningless to talk about 'patches' smaller than the pupil; the only scale picked out is that of the pupil itself.

The statistically independent components that contribute to the scintillation are in fact the many turbulent elements comparable in size to the telescope aperture that are encountered along the line of sight. This aspect of the problem was overlooked in the pre-Kolmogorov days, because astronomers had oversimplified their mental model of the atmosphere to a single layer [phase screen] in the atmosphere. In fact, many regions of the atmosphere contribute to scintillation.

As the variance approaches zero, a log-normal distribution becomes indistinguishable from a Gaussian. Therefore, very weak scintillation always has a nearly Gaussian intensity distribution. This is not due to averaging or 'statistically independent patches' but is a property of the log-normal distribution itself. A practical consequence is that significant tests for log normality can only be conducted when the intensity variance is moderately large. However, if it is too large, the assumption of 'small' perturbations that underlie the derivation of the log-normal distribution is violated; the distribution is no longer log normal in the saturation regime. Therefore, the log-normal distribution can really only be verified in a rather restricted range of intensity variances around perhaps 0.1 or 0.2: much less, and the distribution is sensibly Gaussian; much more, and we enter the saturation regime.

The literature on optical intensity fluctuations in general random media (e.g., Strohbehn et al. 1975), contains many specialized theoretical descriptions, dependent on whether the observer is inside the turbulent medium, or some distance away from a scattering layer; whether one is in the region of weak fluctuations, or in the saturation regime. In the latter case (which in stellar scintillation occurs at great zenith distances), the log-normal distribution cannot remain valid, and a treatment of multiple-path and multiple-scattering effects is required, with both additive and multiplicative effects being important.

The first experimental evidence for log-normal statistics in optical propagation through weak turbulence was obtained by Gracheva and Gurvich (1965) who observed a light

source over long horizontal paths; confirmed for small receiving apertures (but not larger ones) by Fried et al. (1967).

### 5.2 Previous Stellar Observations

When photoelectric recordings of stellar scintillation became possible, a number of authors (e.g., Ellison and Seddon 1952) noted sudden increases of intensity, with durations on the order of 10 ms. The existence of such 'flashes' demonstrated that the statistical distribution of stellar irradiance is far from Gaussian. Such 'spikes' are prominent in small telescope apertures ($\lesssim$10 cm). When $\sigma_I^2$ exceeds a few tenths, spikes in $\Delta I/I$ reach unity some percent of the time.

Several authors quote Jakeman et al. (1978) for the 'confirmation' of log-normal statistics in stellar scintillation. However, the authors in that paper themselves stress the poor observational basis for such a conclusion! While some of their results (at small zenith angles) are consistent with the log-normal distribution, other results for a large zenith angle are not.

Quantitative determinations for stellar scintillation at a low-altitude site were made by Jakeman et al. (1976) for large zenith distances, using a small aperture, and a narrowband filter. Under rather similar conditions, Parry and Walker (1980) measured the first five statistical moments of the intensity fluctuations. For modest scintillation amplitudes, these were consistent with a log-normal model, but for greater ones, departures occurred. Now, the moments approached those for the $K$-distribution, a function often used to model strong scintillation on horizontal paths.

Parry and Walker (1980) found that observing runs yielding approximately the same normalized intensity variance, also gave similar third, fourth, and fifth normalized moments, irrespective of atmospheric condition or zenith angle. This suggests that the dependence of the moments on zenith angle and atmospheric conditions is via *one* parameter only.

Dainty et al. (1982) studied up to the sixth statistical moment, as function of the variance, observed at Mauna Kea and a few other sites. The higher moments were always slightly smaller than those predicted by the log-normal distribution. However, given the integration over space, time, and wavelength, the authors concede that the underlying probability function could still be log normal. In analogous analyses, Stecklum (1985) generally found good agreement with the log-normal expectation, although cases with slightly smaller moments were also observed. The deviations from log normal appeared to increase with increasing zenith distance.

### 5.3 Statistics Measurements on La Palma

Probability distribution functions were extensively recorded during both our winter and summer campaigns. Submillisecond sample times were used and, whenever possible, chosen to give a reasonable average number of counts per sample interval, $\langle n \rangle$, typically around 5 or 10. The integration time was normally 100 s, and the subsequent measurement was normally begun some 20–30 s after the conclusion of the previous one. In winter, many observations were made of Polaris (at almost constant zenith distance $Z \simeq 60°$), while in summer stars in various parts of the sky were monitored.

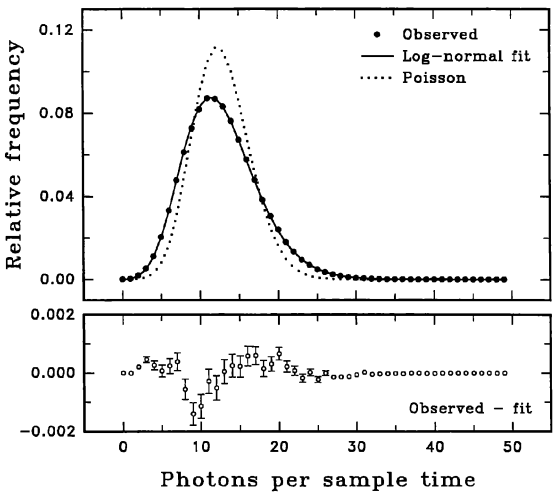


FIG. 2—A typical observed photon-count distribution. A log-normal intensity distribution (combined with appropriate photon noise) is fitted to the data, with the difference to the fit seen in the bottom panel on a greatly expanded scale. The Poisson distribution corresponding to photon noise only, with zero atmospheric intensity fluctuation, is also shown.

Figure 2 shows a representative photon-count distribution (one among hundreds of similar ones), as observed on La Palma, with a superposed fit of a log-normal distribution. This particular summer measurement of *Vega* at zenith distance $Z \simeq 31°$ used an aperture of diameter ∅5 cm; a λ 550 nm filter with $\Delta\lambda = 70$ nm; sample time $\Delta t = 200$ μs; integrating for 100 s; PMT counts per second ≃64,000. The fitted log-normal function gives an intensity variance $\sigma_I^2 \simeq 0.058$.

### 5.4 Variance Determination

#### *5.4.1 Observed Distributions*

The measured probability distributions arise from a combination of the atmospheric fluctuations with the Poisson distribution of the photon counts (inherent in the detection process; e.g., Saleh 1978). Our first use of these distributions is in determining the intensity variance $\sigma_I^2$.

From the probability distributions, the variance was estimated using two different methods: (a) factorial moments, without assuming any specific statistical distribution, and (b) maximum likelihood, assuming a log-normal one. Within the error limits, both methods gave the same variance. We fitted log-normal functions to all our probability distributions (hundreds of measurements under different conditions), finding them to adequately describe measured distributions for $\sigma_I^2 < 0.4$, the range of our measurements. The values of $\sigma_I^2$ used below originate from such fits. Our measuring precision is such, that plausible errors that could originate from the actual distribution being not exactly log-normal are negligible, compared to temporal changes in the atmosphere between successive measurements (≃2 min apart). Typically, the measurement sample size, and the precision of log-normal fitting permit $\sigma_I^2$ to be determined with three or four significant digits, while typical atmospheric changes between mea-

surements appear already in the second digit. Occasional deviations from log-normal distributions anticorrelate with the quality of the data: strong discrepancies could be identified as being due to the appearance of clouds, errors in guiding, etc.

Assuming that the intensity fluctuations are not undersampled, the variance can *also* be determined from autocorrelation measurements (described further below), by extrapolating that function to zero time lag. One advantage with autocorrelations, is that these are less affected than probability distributions by detector dead time and afterpulsing (Appendix). Another advantage is that they give stable values also in situations with very low count rates (e.g., for very small telescope apertures). Where directly comparable data were available, these two methods were found in good agreement.

#### *5.4.2 Simulated Distributions*

For comparing with observations, synthetic photon-count histograms were computed, by numerically simulating the Poissonian detection process of a log-normally varying signal. Two methods were tried, which in theory should be equivalent; in practice the first one is much too slow to be useful and was only used as a validation of the second, more efficient method.

The first method is very direct: for each of the $N$ samples, an independent log-normal variate was first generated [$I=\exp(\mu+\sigma_I x)$, where $x$ is a normal variate with expectation 0 and variance 1, and $\mu$, $\sigma_I$ are constants], and then a Poissonian deviate $n$ with expectation $I$. Standard numerical routines were used, with special attention to the random-number generator—several different ones were tried. Then the $N$ independent realizations of $n$ were collected in a histogram, the factorial moments computed, etc. A disadvantage of this method is that the computing time is proportional to $N$, and also that very many random numbers must be generated (at least two for each sample), with a risk to encounter some effects of the finite random-number sequence.

The second method first calculates the probabilities p($n$) as the marginal distribution of p($n|I$)=(product of Poisson and log-normal densities). Then, the histogram is simulated as a multinomial distribution of the $N$ samples. This is done recursively as a sequence of binomial distributions, each conditional on the histogram bins already simulated. This method is much more efficient because the execution time is largely independent of $N$.

### 5.5 Skewness and Excess

Although log-normal fits do closely agree with observations, there are subtle but systematic differences, readily seen already after a short measurement (Fig. 2). To closer examine the scintillation statistics, we now turn to the higher statistical moments. The information one can hope to get concerns global properties of the probability distribution, like its width, shape, and asymmetry.

Let $h(n)$, $n=0,1,2,...,63$, be the data of the probability distribution histogram, i.e., $h(n)$ is the number of sample-time intervals with exactly $n$ counts per sample. The total number of measured sample-time intervals equals $N$. The $k$:th moment of the intensity is estimated as the $k$:th factorial moment of the photon counts (which allows for the effect of the Poisson distribution's smearing the underlying intensity distribution; e.g., Cummins and Pike 1974):

$$\langle I^k\rangle=\langle n(n-1)(n-2)...(n-k+1)\rangle$$

$$=N^{-1}\sum_{n=k}^{\infty} n(n-1)...(n-k+1)h(n) \qquad (5)$$

and the normalized moments $m_k$ are

$$m_k=\langle I^k\rangle/\langle I\rangle^k=\frac{\langle n(n-1)...(n-k+1)\rangle}{\langle n\rangle^k}, \quad k=2,3,\ldots . \qquad (6)$$

From the normalized moments of order $k=2$ to 4, the following are computed:

$$\sigma_I^2=m_2-1 \quad \text{(variance)}, \qquad (7)$$

$$\gamma_1=(m_3-3m_2+2)/\sigma_I^3 \quad \text{(skewness)}, \qquad (8)$$

$$\gamma_2=(m_4-4m_3+6m_2-3)/\sigma_I^4-3 \quad \text{(excess=kurtosis)}. \qquad (9)$$

The skewness and excess are defined with reference to a normal (Gaussian) distribution, where $\gamma_1=\gamma_2=0$.

Because the variance $\sigma_I^2$ obviously changes between different observations, we must look for a family of distributions depending on at least one parameter (apart from the scaling factor $\langle I\rangle$), corresponding to the relative width of the distribution. If this family depends on only one such parameter, and there is a one-to-one relation between that and $\sigma_I^2$, then the skewness and excess are also uniquely determined by that parameter and hence by $\sigma_I^2$. The log-normal distributions form an example of such a family. In the log-normal case the relations between $\sigma_I$, $\gamma_1$, and $\gamma_2$ are

$$\gamma_1=3\sigma_I+\sigma_I^3, \qquad (10)$$

$$\gamma_2=16\sigma_I^2+15\sigma_I^4+6\sigma_I^6+\sigma_I^8. \qquad (11)$$

A first test of the log-normal hypothesis is therefore to plot the observed skewness and excess versus $\sigma_I$ and $\sigma_I^2$, to see whether they follow these relations. This was done for all histograms with positive variance, recorded in both the winter and summer campaigns. The conclusions:

(a) The intensity distribution tends towards normality (or at least $\gamma_1=\gamma_2=0$) when $\sigma_I^2\to 0$.

(b) Although the skewness and excess are in general positive, they are on average *significantly smaller* than expected for log-normal distributions with the same $\sigma_I^2$. This agrees with previous findings by Dainty et al. (1982) and Stecklum (1985).

(c) Apart from statistical noise, it appears that the skewness and excess are unique functions of the variance. One has approximately

$$\gamma_1\simeq 2.75\sigma_I, \qquad (12)$$

$$\gamma_2\simeq 12\sigma_I^2. \qquad (13)$$

This indicates that all data may be consistent with a single family of distributions. A number of representative measurements were examined to see whether some other distribu-

tions proposed in the literature could give a better representation of the observed moments, concluding:

(a) *Normal (Gaussian) distribution* is clearly rejected because the skewness and excess are generally positive.

(b) *Log-normal distribution* is also rejected because it gives too much skewness and excess.

(c) *Gamma (chi-square) distribution* is rejected because it predicts a skewness and excess which are smaller than observed. In fact, the observations typically fall about midway between the log-normal and gamma distributions.

(d) *Beta distribution of the second kind (F distribution*; e.g. Kendall and Stuart 1977). This family depends on two distribution parameters $\alpha$ and $\beta$, which can be adjusted to the observed $\sigma_I$ and $\gamma_1$ provided that $\gamma_1 \geqslant 2\sigma_I$. For small $\sigma_I$, we have $\gamma_1 \propto \sigma_I$ and $\gamma_2 \propto \sigma_I^2$ if there is a fixed ratio between $\alpha$ and $\beta$, $\eta = \beta/\alpha$. Depending on $\eta$, the $\sigma_I - \gamma_1$ and $\sigma_I^2 - \gamma_2$ relations fall between the gamma distribution (to which the beta distribution reduces for $\eta = 0$) and the log normal (which it resembles for $\eta \simeq 0.7$ to 1.0). A rather good fit to observations, both in skewness and excess, can be obtained for $\eta \simeq 0.3$.

(e) *I-K distribution* (Andrews and Phillips 1985) is also a two-parameter family. A reasonable skewness may be obtained, but the excess is always too large.

Of the distributions considered, the *F* distribution (or beta distribution of the second kind) is thus the only one which matches the observed moments (up to fourth order) reasonably well. However, we have no *physical* arguments for the use of this distribution: it was tested only as a mathematical hypothesis.

The preceding analysis shows that the interpretation of the statistical moments in terms of an intensity distribution is far from obvious: it may permit us to reject certain distributions, but does not tell what the real distribution is. There is obviously a danger that one tends to accept as 'real' the first distribution that happens to fit the first few observed moments. One way around such a 'prejudiced' analysis would be to calculate the distribution itself by numerical inversion of the measured probability histogram. A number of numerical experiments of this kind were made. Comparing the results of such inversions of observed data, checking the noise levels and reproducibility with simulated data, showed that the deviations from log-normal are real and not caused by the inversion process.

### 5.6 Log-Normal Moments not Unique

A straightforward approach to studying a probability distribution, practiced by many, is to calculate the moments of intensity. However, while many statistical distributions are uniquely determined by their moments, this is *not* true for the log-normal one, whose moments are

$$\langle I^k \rangle = \exp[k(\langle \ln I \rangle + \tfrac{1}{2} k \sigma^2_{\ln(I)})]. \quad (14)$$

There are other distributions which possess the same moments as the log-normal one (Strohbehn et al. 1975; Barakat 1976). Some (but not all) authors have been aware of this limitation: by comparing moments, it is possible to show consistency with, but not to prove that intensity fluctuations are indeed log normal (e.g., Dainty et al. 1982; Parry and Walker 1980). There are consequences for some theoretical approaches: any theory that predicts a log-normal distribution on the basis of intensity moments must be suspect. For a more general discussion on this uniqueness question, see Majumdar (1984).

When statistical moments are not adequate, hypothesis testing and goodness-of-fit tests may be used (Strohbehn et al. 1975). To decide whether data best fit a log-normal or another distribution, maximum likelihood estimates can be used to first determine the parameters of each candidate distribution which make it best fit the data. Then, the second step is to compare the different hypotheses, selecting the one with the maximum probability of fitting.

### 5.7 Can Scintillation Statistics be Determined at All?

Irrespective of whether the mathematics permit the unique determination of a certain distribution, there are observational issues. A practical one is that the higher moments of irradiance may be distorted because of detector saturation or dead-time effects (Hill and Churnside 1988; Appendix). To circumvent such effects, it seems safer to compare theoretical and measured probability distributions (where the affected intensity bins can be identified), than to compare their moments. To avoid detector/amplifier saturation requires systems with a *very* wide dynamic range. Measurements of e.g., the fifth moment of a signal with a large log-normal component may require a saturation limit of several hundred to a thousand times the mean signal. At the same time, the signal needs to be known accurately, since its fifth power is used for normalization. The total dynamic range required could easily be as large as $10^5$.

A more fundamental observational problem is that an enormous number (millions) of independent samples are needed in order to obtain statistically significant determinations of higher moments (Ben-Yosef and Goldner 1988; Frehlich and Churnside 1989; Goldner and Ben-Yosef 1988; Hill and Churnside 1988). These authors argue that, for reasonable and practical sample sizes, the correct estimation of such values is improbable or even impossible.

The limitation lies not in amassing such quantities of data, but in the nonstationarity of the atmosphere. In sampling its properties, one has to assume that the underlying statistical process does not vary during the observation time.

The sample size is limited by the length of time in which the atmospheric turbulence remains stationary. With a correlation time of $\simeq$10 ms, one has a maximum of $\simeq$100 uncorrelated samples per second. With wind-velocity fluctuations, the refractive-index structure constant changes, and the irradiance moments must also fluctuate. Such changes will affect the apparent deduced higher moments in longer time series. If stationary conditions do not exceed $\simeq$100 s, most results will be limited by a maximum intensity of perhaps ten times the average: there is no time to await the rare [but significant] thousandfold-intensity peak. Since higher moments $m_k$ are strongly dependent on such rare events, the finite integration time usually causes such moments to be underestimated. From numerical simulations, Frehlich and Churnside (1989) show how the effects of amplifier saturation become signifi-

cant when the saturation irradiance is less than the median of the maximum irradiance value for a given sample size $N$, and a model PDF.

The interpretation of experimental results is further confused by the fact that both $m_k$ and the variance $\sigma_I^2$ are usually measured from the same data, so that both fluctuate correlatively (in theoretical calculations $\sigma_I^2$ is an independent variable, and $m_k$ is calculated from the PDF). In passing, we also note that the strongly non-Gaussian character of scintillation violates the usual assumptions made in least-squares and error analyses, often applied to fitting observational data.

With 100 independent samples per second, there are on average $10^4$ s ($\simeq$3 h) between observations of irradiance events having a $10^{-6}$ probability. Since statistically stationary atmospheric conditions are hardly longer than that, efficient observational methods have to be found. This conflict between required sample size and nonstationary atmospheric conditions was already felt by previous observers (e.g., Bufton and Genatt 1971; Dainty et al. 1982). Suggested compromises include to sample [much] faster than ideally would be correct in order to obtain truly independent samples (Hill and Churnside 1988).

There may be other solutions. A large number of stars could (at least in principle) be observed simultaneously, yielding additional information as an ensemble of statistical distributions. There may be practical issues concerning the plethora of experimental equipment required (numerous telescopes and detectors, or perhaps multiple-object photometers on wide-field telescopes). One limitation will come from the finite number of sufficiently bright [natural] stars available within a certain limited area of the sky, where scintillation can be expected to be statistically similar. However, irrespective of the above issues, there is always the possibility of studying a large number of consecutive shorter measurements: one will then obtain the temporal *statistics* of statistical fluctuations: we will follow such a track in the present work.

Figure 3 shows this nonstationarity of the atmosphere, exemplified by the aperture dependence of the variance $\sigma_I^2$. These summer observations of Vega at $\lambda$ 550 nm were made as a rapid sequence for apertures between 1.2 and 20 cm at zenith distances $Z\simeq30°$, repeated 'one hour later' at $Z\simeq17°$. The variances were obtained by fitting log-normal distributions to probability distribution histograms, as described above. The main point here is to illustrate that, although the scintillation amplitude changes significantly, the *functional law* for—in this case—the aperture dependence, appears to remain largely unaffected. This suggests that, even though the atmosphere changes all the time, its long-term ensemble average of rapid fluctuations may be a stable function, open for determination.

In Fig. 3 one notes how the scintillation amplitudes become essentially independent of aperture size for $D\lesssim5$ cm, where the structures in the 'flying shadows' in the pupil plane appear to be resolved. The epoch 'one hour later' corresponded to a period of good seeing in the sense of high speckle contrast and a small number of speckles (cf. Figs. 5 and 13).

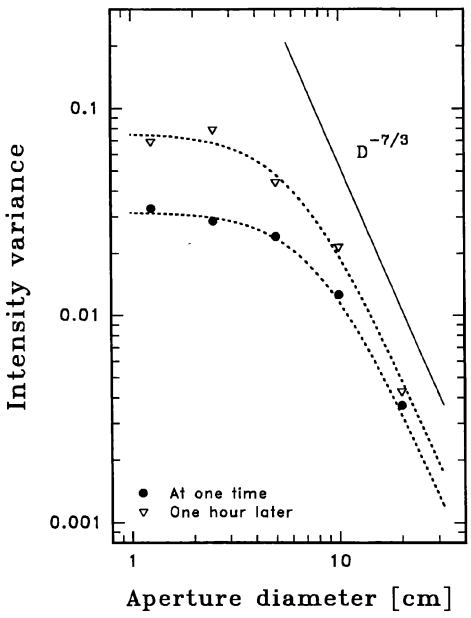


FIG. 3—Aperture dependence of the intensity variance $\sigma_I^2$, measured at two different times during the same night. The marked slope $-7/3$ corresponds to Eq. (2), the expected behavior for large apertures. This figure illustrates how the functional law for the aperture dependence of scintillation remains unaffected by changes in scintillation amplitude. The data points correspond to those in the analogous Fig. 5 for autocovariance.

### 5.8 Higher-Order Statistical Moments

As seen above, high-quality data do reveal subtle but systematic differences between observed distributions and those expected from log-normal intensity fluctuations. In Sec. 5.5, the lower statistical moments (of order $k$=2 to 4) were treated, and now we will examine also the higher ones ($k$ up to 12). There may exist astronomical sources, for which such higher moments of intensity variation convey unique information, and thus one will need to accurately disentangle atmospheric effects.

The measurement of higher-order moments can be quite challenging. Any credible determination requires not only adequate measurement statistics, but also an understanding of the noise characteristics and biases that result from finite sampling sequences. Here, we do not aim for any systematic study of different atmospheric conditions, apertures or zenith distances. Rather, we want to examine how far observational and data reduction techniques can be extended, using representative data. A number of measured histograms were selected to compute statistical moments, comparing these with numerical simulations.

Numerically simulated observations were used to study the effects of, e.g., increased amounts of data. In one sequence, the average number of photon counts per sample time $\langle n\rangle$ was varied, in another the total number of sample-time intervals $N$ was increased from 100 to $10^9$. In our data, a typical 100-s integration with sample time $\Delta t$=100 $\mu$s, implies $N=10^6$.

For these high-order statistics, where subtle trends are to be extracted from very large samples, one must assure that the random number generator passes various tests for 'clean-

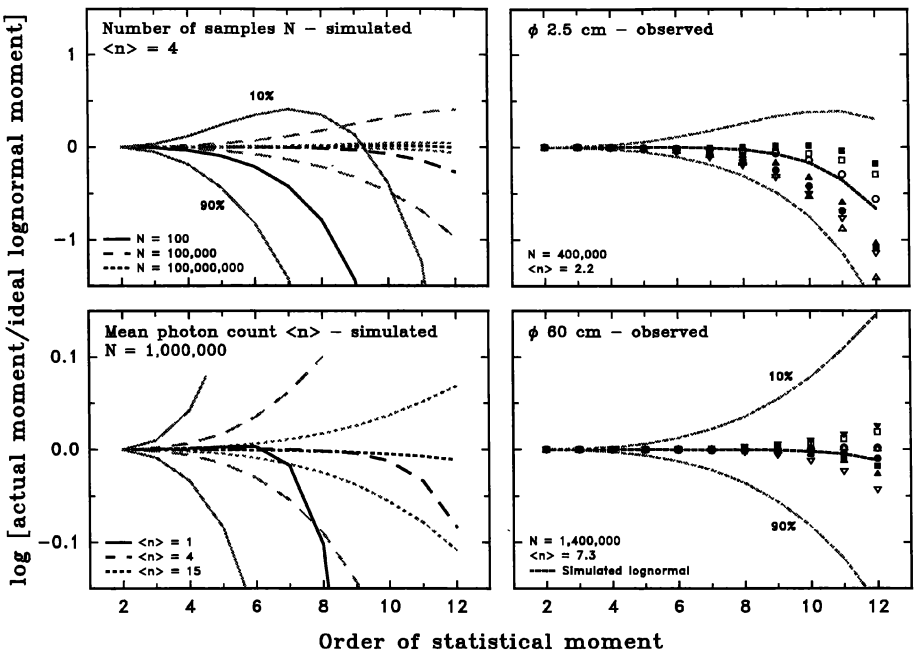


FIG. 4—Higher-order statistical moments ($m_k$ of order $k$) in atmospheric intensity scintillation, and problems in their determination. At left are shown numerically simulated observations: effects of increasing the number of photon count samples $N$ (top), and average counts per sample time $\langle n \rangle$, keeping the autocovariance constant=0.14. The noise naturally decreases with an increasing number of samples $N$ (top left), and for fixed $N$ it decreases with increasing $\langle n \rangle$ (bottom left). The distribution of the moments, as obtained from many simulations, defines the median (bold), and the 10% and 90% percentiles (shaded). The quantity plotted is $R_k = \log_{10}\{m_k(\text{actual})/m_k(\text{ideal})\}$, where the actual value is that obtained from either simulations or observations, and the 'ideal' is that analytically computed for a log-normal distribution with the observed variance. $R_k$ approaches 0 for long simulation series. In shorter measurement series, however, bias phenomena appear due to the finite number of samples. At right, representative observations are compared to simulations for relevant $N$ and $\langle n \rangle$, demonstrating how the average values (but not their statistical spread) of higher-order statistical moments are consistent with log-normal distributions.

liness.' Three different random-number generators were examined (#1, #2, and #3). Two are based on the well-known principle of shuffled linear congruential sequences, while the third is based on a subtractive method.

Since it appeared likely that these three generators (from reputable software suppliers) would pass most 'ordinary' statistical tests, and an extensive analysis of their properties was outside our scope, they were tested by running the simulations through the data reduction chain. It turned out that #1 gave significantly deviant results, and was abandoned. The differences between #2 and #3 were more subtle. Both gave a similar spread in the higher normalized moments, but the fiftieth percentile from #2 (in the format of Fig. 4) seemed to stick more closely to the zero-level than for #3. Based on this, and the fact that the mathematical principle behind #2 is better understood than that of #3, the choice fell on the former. Since #2 and #3 are based on quite different mathematical principles, but give very similar results, we believe that the features discussed below are real and not due to inadequate random numbers.

For each set of parameters, 5,000 probability distribution histograms were numerically produced. The starlight intensity was assumed to be log-normally fluctuating, subject to a random (Poisson) photon detection probability. From these histograms, the statistical moments were computed, and their distribution, in particular the median, and the 10% and 90% percentiles (thus confining an 80% confidence interval). Results are shown in Fig. 4, where such medians are the bold curves, while the 10% and 90% limits are shaded.

To facilitate an inspection of the statistical moments $m_k$ of order $k$, the quantity plotted in Fig. 4 is $R_k = \log_{10}\{m_k(\text{actual})/m_k(\text{ideal})\}$, where the 'actual' value is that obtained from either simulations or observations, and the 'ideal' that analytically computed for a log-normal distribution with the same variance. The *observed* variance was used both in computing the 'ideal' log-normal moments, and in normalizing the higher ones, both for observations and simulations (rather than the population variance, which would have introduced a wider spread in $R_k$; as a consequence, $R_1 \equiv R_2 \equiv 0$). When the 'actual' and 'ideal' moments are equal, $R_k = 0$, a value approached for long simulation series. For finite series, however, a number of nontrivial bias phenomena appear.

Most noticeable among these is the asymmetry of the median curve for moments of high order, with a decrease below the 'ideal' values. The origin of this phenomenon can be traced to the method of calculating the statistical moments from the observed photon-count distribution. The $k$:th *factorial moment* $\langle n(n-1)(n-2)\ldots(n-k+1) \rangle$ of the photon counts $n$ equals the $k$:th ordinary moment of the intensity distribution. In a photon-count distribution based on a finite number of samples there is a certain maximum value to the counts per sample time, $n_{\max}$. It follows that all calculated moments of order greater than $n_{\max}$ are strictly zero. The

simulations show that also other moments of order below $n_{max}$ are statistically influenced by this effect and, on the average, take on values less than the 'ideal' ones. The effect is somewhat analogous to that of fitting a polynomial of successively higher degree to a fixed number of data points: the residual between the fit and the data ultimately becomes zero although the underlying function is still not correctly described. Although this effect of the limited number of samples must be generally present in analyses of photon-count distributions, we are not aware of previous discussions of this effect in the literature.

In the right-hand panels of Fig. 4, representative observations are compared to simulations. For the 2.5 cm aperture, the mean $\sigma_I^2$ was 0.28. These λ 550 nm observations of Vega at zenith distance $Z \simeq 17°$ had $\Delta t = 230$ μs; $\langle n \rangle = 2.2$; integrating 90 s for each of the eight measurements. The stable summer weather on La Palma was characterized by a steady northerly wind. The 60 cm observations of Vega were made the same night, λ 400 nm; $\sigma_I^2 = 0.054$; $Z \simeq 15°$; $\Delta t = 70$ μs, $\langle n \rangle = 7.3$; integrating for 100 s.

The observed data do center around the curve expected for log-normal distributions. However, the data points scatter much less about the mean than expected for log-normal distributions. This becomes especially pronounced for larger entrance apertures (and smaller scintillation amplitudes). For a log-normal distribution, one would have expected that 20% of the data points would fall outside the 10% and 90% percentiles: the actual fraction is very much less.

The sample time used in the observations was rather shorter than the characteristic coherence time of scintillation. Consequently, the number of 'independent' intensity values is rather smaller than the total number of samples. This should tend to *increase* the scatter of the observed higher moments, compared to simulations, where each sample is assumed to be statistically independent. The discrepancy between the observed and simulated scatter is thus even greater than it appears from Fig. 4.

At this time, we cannot yet offer a full explanation for this behavior. Some aspects of the measured statistics are consistent with log-normal behavior, while others are not. There exist further uncertainties in these simulations. One factor is that the random numbers generated do not carry any 'memory' of previous numbers. This differs from real scintillation, where there is an anticorrelation between intensities observed some time apart. That is caused by the conservation of energy: focusing of light into a bright spot somewhere requires there to be a darker spot somewhere else. However, no such physical requirements of energy conservation entered the simulations: whether this could have any significant effects is not clear.

In any case, our discussion illustrates how even statistical moments of a quite high order actually can be measured and analyzed. Although the atmosphere undergoes rapid changes, the *ensemble* of measured probability distributions defines a statistical sample which can be tested against simulations.

Nevertheless, given that higher-order moments can be strongly affected by just a few data points with extreme values, one must wonder whether some rare outlier points, perhaps not fully measured (due to dead-time or other effects), could account for the diminished spread in the observed moments. It is awkward to accurately calculate such detector effects, which may depend on actual count rates, previous illumination history, cosmic-ray events, etc. Such subtle effects are likely to ultimately limit the accuracy in interpreting these types of data (Appendix). In order to further explore the structure of scintillation, we now turn to temporal correlation functions, whose measurements seem largely unaffected by such detector effects.

## 6. AUTOCORRELATIONS AND THEIR TEMPORAL CHARACTERISTICS

In this section, we will examine representative functions for the temporal correlation of stellar intensity fluctuations, their reproducibility between different epochs, and their structure over 'all' measurable time scales.

The autocovariance ACV($\tau$) of intensity $I(t)$ measures the average strength of the relative intensity fluctuations $[I(t) - \langle I \rangle]/\langle I \rangle$ for different time delays $\tau$. If the windspeed is known, the ACV indicates structure sizes in the flying-shadow pattern. The limiting values for short and long delays are ACV(0) = $\sigma_I^2$ and ACV(∞)=0. The auto*correlation* function ACO($\tau$)=ACV($\tau$)/ACV(0) equals unity at delay zero.

### 6.1 Data Reduction

The autocovariance function is defined as

$$\mathrm{ACV}(\tau) = \frac{\langle I(t) I(t+\tau) \rangle}{\langle I \rangle^2} - 1. \qquad (15)$$

The number of photons $n(t)$ detected in the interval $[t - \Delta t/2, t + \Delta t/2]$ provides an estimate of $QI(t)$, whenever the sample time $\Delta t$ is much shorter than the time scales of intensity fluctuations; here, $Q$ is a constant factor depending on the intensity unit used, the length of the sample-time interval, the quantum efficiency of the detection process, etc. Assuming $n(t)$ to be a Poisson process with mean $QI(t)$, we have $\langle n \rangle = Q\langle I \rangle$ and, for non-overlapping samples ($|\tau| \geq \Delta t$), $\langle n(t) n(t+\tau) \rangle = Q^2 \langle I(t) I(t+\tau) \rangle$. Inserting this in Eq. (15), $Q$ cancels, and the ACV of $I(t)$ can be estimated as the ACV of $n(t)$,

$$\mathrm{ACV}(\tau) = \frac{\langle n(t) n(t+\tau) \rangle}{\langle n \rangle^2} - 1 \qquad (16)$$

(e.g., Cummins and Pike 1974; Jakeman and Pusey 1980). This expression is used to calculate the ACV for $\tau = \Delta t$, $2\Delta t, \ldots$ .

For $\tau = 0$, Eq. (15) gives the intensity variance $\sigma_I^2$. Equation (16) must in this case be modified to take into account the contribution to $\langle n^2 \rangle$ due to photon noise. For a Poisson process, $\langle n(n-1) \rangle = Q^2 \langle I^2 \rangle$, and the variance becomes

$$\sigma_I^2 = \mathrm{ACV}(0) = \frac{\langle I^2 \rangle}{\langle I \rangle^2} - 1 = \frac{\langle n^2 \rangle}{\langle n \rangle^2} - \frac{1}{\langle n \rangle} - 1. \qquad (17)$$

The ACV function can also be obtained in a cross-correlation mode, taking the counts $n_1(t)$ and $n_2(t)$ from different detectors, measuring the same signal following a beamsplitter. In this case

$$\mathrm{ACV}(\tau)=\frac{\langle n_1(t)n_2(t+\tau)\rangle}{\langle n_1\rangle\langle n_2\rangle}-1 \qquad (18)$$

for any $\tau$ (including $\tau=0$).

In practice, ACV measurements were not made for delay zero. ACV(0) may instead be obtained from the photon-count histogram, as described in Sec. 5.5, or (better) by extrapolating the measured ACV($\tau$) to $\tau=0$.

### 6.2 Clipped Autocorrelation

To simplify the signal processing, our computed correlation functions are *clipped* ones, i.e., at any time lag, the contribution to the function is given by multiplying $n(t+\tau)$, the actual number of photon counts, with $n_{\mathrm{clip}}(t)$ which takes the value of either 0 or 1, depending on whether $n(t)$ was below, or did reach or exceed a preset clip level. A thus clipped correlation function (with ideal clip level=$\langle n\rangle$) is equivalent to the full correlation function in the case of a randomly varying (Gaussian) signal, the only difference being a somewhat increased noise level (e.g., Saleh 1978). Such clipped correlation functions are, of course, widely used in light scattering experiments.

The clipped autocorrelation function at delay $\tau$ is computed as

$$\frac{\langle n_{\mathrm{clip}}(t)n(t+\tau)\rangle}{\langle n_{\mathrm{clip}}\rangle\langle n\rangle}-1, \qquad (19)$$

where $\langle n_{\mathrm{clip}}\rangle$=average number of clipped events during one sample-time interval. By normalizing this function to the intensity variance at $\tau=0$, ACV($\tau$) is obtained. To estimate $\sigma_I^2$ from this clipped autocorrelation, we use an iterative process:

(a) Assume a log-normal distribution for the intensity fluctuations.

(b) Estimate a starting value for the variance $\sigma_I^2$.

(c) Extrapolate ACV($\tau$) to $\tau=0$. This gives the 'measured' value of $\langle n_{\mathrm{clip}}(t)n(t)\rangle$, excluding photon noise.

(d) Compute the theoretical $\langle n_{\mathrm{clip}}(t)n(t)\rangle$, and then iterate a number of steps until converging to a value of $\sigma_I^2$.

### 6.3 Transforming to Power Spectra

Measured autocovariances were also transformed to *power spectra* (the ACV and the power spectrum are integral transforms of each other). The power spectra are normalized to satisfy $\int_0^\infty P(f)\,df=\sigma_I^2$, i.e., the integral over frequency $f$ of the power spectral density $P(f)$ [Hz$^{-1}$] equals the normalized variance $\sigma_I^2$. Figure 7 is our first to show such a *power spectral density* (PSD).

In practice, to find the optimum transformation to PSD of the desired frequency range and resolution can be nontrivial because of incomplete sampling and noise in the ACV functions. In principle it may be computed as the cosine transform of the autocovariance function. However, in the presence of noise, there is no guarantee that the cosine transform of the measured ACV is non-negative at all frequencies. This is in contrast with another method of PSD estimation, taking the square of the modulus of the Fourier transform of a time series of intensity measurements: then the PSD must be non-negative. One probable advantage of the method used here (going via the ACV) is that the calculated PSD should be unbiased by any white-noise component of the intensity measurements, such as photon noise.

Such a direct transform of an ACV with equidistant samples yields a number of *discrete* data points defining the power spectrum: these are the *points* plotted in, e.g., Fig. 16.

When the autocovariance consists of unequally spaced data (as obtained by putting together measurements with different delays), it must be interpolated to the smallest delay step before transforming. Several mathematical manipulations were tried, e.g., 'optimally' smoothing the autocovariances with cubic splines before transforming (which seems to improve the high-frequency part of the PSD). The PSD functions obtained from smoothed ACVs are in a sense *continuous* estimates, and such functions are therefore plotted as continuous lines.

Some plots also show the *power content*, $P(f)\cdot f$. While $P(f)$ gives the scintillation power per frequency interval, $P(f)\cdot f$ shows which frequencies contribute most scintillation power. A constant interval in $\log f$ corresponds to a frequency interval proportional to $f$, and $P(f)\cdot f$ plotted on a logarithmic scale thus shows the distribution of variance over [equally large] intervals in $\log f$.

The ACVs and PSDs are mathematical transforms of each other, and in principle would appear to contain equivalent information. In practice, that is not the case, due to their different noise properties (e.g., noise in power spectra often has a 'spiky' appearance).

The main difference, however, is that our power spectra do not extend to especially high frequencies, although there are good ACV measurements on time scales down to 1 $\mu$s, say. To compute a corresponding power spectrum up to 1 MHz in frequency, would have required a 1 $\mu$s resolution *throughout* the delay range, not only for shorter delay times. The time resolution that can be fully utilized for power spectra equals (maximum delay)/64, due to the design of our 64-channel correlator. Since a full correlation curve up to perhaps 30 ms delay must be included for the transform, the maximal resolution becomes some 0.5 ms, sufficient for a power spectrum only up to $\simeq$1 kHz.

In principle, this limitation can be circumvented: one could, e.g., fit an autoregressive time-series model to the observed data, and then compute the power $P(f)$ as a rational function. The problem with this method seems to be that it tends to squeeze in most of the variance in a narrow frequency band, corresponding to that cosine function, which best represents the peak of the ACV. Such a method (and its problems) are analogous to maximum-entropy ones.

### 6.4 General Properties and Typical Time Changes

Although the general appearance of the autocorrelation function is highly repeatable, systematic changes often occur over periods of tens of minutes, leading to different function shapes. Figure 5 shows two sequences with qualitatively different types of autocorrelations, resulting from observing *Vega* at different times during the same summer night. The left panel (a) shows measurements in the evening at moderate zenith angles ($Z\simeq30°$), and (b) 'one hour later' those

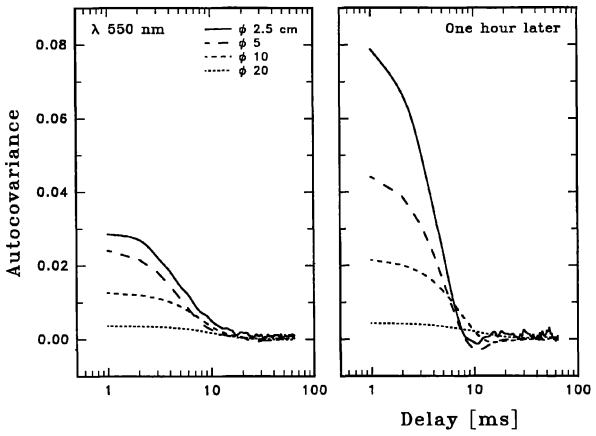


FIG. 5—Aperture dependence of autocovariance functions, measured at different times during the same night. Left shows measurements early in the evening at moderate zenith angles; Right 'one-hour later' shows measurements closer to midnight at small zenith angles. The anticorrelation dips on the right indicate a high temporal stability in the flying shadows. Their appearance correlated with times of good seeing in the sense of high speckle contrast and a small number of speckles.

closer to midnight and closer to zenith ($Z \simeq 17°$). These data are for λ 550 nm, sampled with $\Delta t = 1$ ms; integrating for 100 s. Each sequence for apertures of different size took some 20 min to record, and the two were separated by about 75 min in time.

There is a systematic trend, such that greater variances are accompanied with an *anticorrelation dip* in the ACVs. This indicates that the [two-dimensional] flying shadows are then sufficiently regular and long-lived to preserve a pattern of alternating brighter and darker structures in the [one-dimensional] autocovariance function, even after integration and averaging during a few minutes. Small variance is accompanied by a 'smooth' ACV function without any anticorrelation dip. The trend was similar also in measurements at λ 400 nm and (less pronounced) at λ 700 nm.

For smaller apertures ($D \lesssim 5$ cm), the autocorrelation halfwidths ($\simeq 4$ ms) become largely independent of the aperture, suggesting that the spatial [and temporal] structures in the 'flying shadows' on the ground are now resolved. This spatial resolution is also indicated by the second set of curves ('one hour later'). Now there are pronounced anticorrelation dips at delays around 10 ms, at least for the smaller apertures. The aperture size where this occurs is obviously some measure of a characteristic size in this pattern. The amplitudes here continue to increase also for the smaller apertures, apparently indicating the presence of high-contrast structure also on these smaller scales. From simultaneous observations of the stellar speckle images, the time 'one hour later' could be identified as periods of good seeing in the sense of high speckle contrast and a small number of speckles (see further Sec. 10 below).

When the 'flying shadows' are cleaner and have higher contrast, we are probably seeing a shadow pattern that is dominated by a single wind component in the atmosphere, while otherwise there are several. The expected effect of wind shear (different wind velocity vectors at different altitudes), would be to smooth out the fine structure in the correlation functions. An analogous effect is seen for increasingly large apertures. The phenomenon has a marked seasonal dependence: anticorrelation dips were often observed during good summer conditions, but never in winter (cf. Fig. 15).

However, the autocorrelation *time scales* between the epochs of Fig. 5 are unchanged: the speed of motion of the 'flying shadows' is unaffected (unchanged influence from high atmospheric layers?), but the shadows can be interpreted as having more or less sharp edges. Of course, the *spatial* properties of the shadow pattern components are independent of wind velocity and shear, which affect only the *temporal* ones.

At ground level, no obvious meteorological changes were noted which could reasonably explain these changes, which thus must be related to high-altitude turbulence and dynamics. (Although, between these two particular sets of measurements, it was noted that a few small clouds appeared in one part of the sky.) That, between the measurements in Fig. 5, the variance increased more for small apertures than for large ones, could also suggest an increase of turbulence at lower heights than the average in the first sample. A decrease of the mean Fresnel-zone size with a decrease of the distance to the scintillation-producing turbulence would result in more smaller-scale structure in the flying shadows (cf. Young 1969).

A theoretical analysis of [spatial] autocovariance functions and power spectra of stellar shadow patterns is in Roddier (1981; his Chap. 8; his Figs. 12 and 14). Although the assumptions are idealized (e.g., one thin turbulent layer at a given altitude), the calculations are quite illustrative. Patterns displaying large shadows can be attributed to turbulence near the tropopause, whereas smaller ones are produced at low altitude. For $h = 10$ km, his ACV functions have an anticorrelation dip at a spatial lag $\simeq 8$ cm. At a windspeed of 10 m s$^{-1}$ (typical value as measured from correlations in double apertures; Paper III), this corresponds to a time delay $\tau = 8$ ms, close to our measured values.

### 6.5 Time Scales in Previous Studies

A number of authors have studied time scales of scintillation, deduced from autocorrelations or similar functions. On Mauna Kea, Dainty et al. (1982) found a very large spread: the $1/e$-widths of the autocorrelation function varied between 1.7 and 10 ms, with a small-aperture average of 3.5 ms. While similar to observations by Parry et al. (1979), they are shorter than correlation times recorded at some other sites (Stecklum 1985).

Perhaps the earliest observations of 'after-effects' in scintillation, equivalent to anticorrelation dips in autocorrelations, were by Fürth (1956), later seen also by Knoechel and von der Heide (1978) and Zhukova (1958).

### 6.6 Scintillation on its Shortest Time Scales

Most studies of scintillation have been for time scales around its dominant one of $\simeq 10$ ms. The 1000 times slower atmospheric changes (10 s) are often called *variable extinction* or *transparency variations*, and are examined in treatises

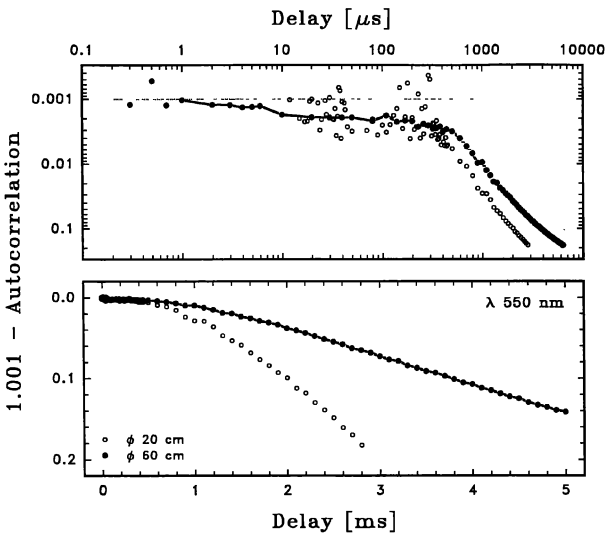


FIG. 6—Stellar scintillation on very short time scales. This plot shows the small deviations from unity of the intensity autocorrelation function close to the origin. The apparent break in the curve near 300 $\mu$s may be connected to the *inner scale* of atmospheric turbulence (linear size $\simeq$3 mm at windspeeds of $\simeq$10 m s$^{-1}$). Photon noise causes a spread of data points for the shortest delays.

on accurate stellar photometry; however quantitative data for 1000 times faster time scales (10 $\mu$s) do not seem to exist in the literature.

The first efforts to study microsecond-scale scintillation appear to have been by Zwicky (1950; best described in Oosterhoff 1957). The time variability was recorded as spatial structure in trailed images of a star, culminating in observing Sirius by rapidly propelling a film across the prime focus of the 200-inch Hale telescope. These star trails showed knots, splits, and lateral excursions.

From a peak around 10 ms, the scintillation power decreases for more rapid fluctuations. How rapid scintillation components still remain measurable, depends on the experimental sensitivity: in our case meaningful measurements down to $\simeq$100 ns were possible. Figure 6 shows the short-delay part of the autocorrelation function, down to 300 ns time lag. On longer (i.e., millisecond) time scales, the ACO function is smoothly and regularly decreasing (cf. Figs. 5 and 7), but at shorter delays there is largely a lack of such behavior, only a slow (perhaps asymptotic) approach towards the origin.

### *6.6.1 Auto- Versus Cross Correlation*

Accurate measurements on the shortest time scales requires particular attention to instrumental effects (see Appendix). *Auto*correlation data from a single photomultiplier begin to get affected by afterpulsing or similar effects at delay times below some $\mu$s. To circumvent this, all data for shorter delay times ($\tau \leqslant 2$ $\mu$s) in Figs. 6 and 7 are instead *cross* correlations, where the photon pulses from one detector have been correlated with those from another, measuring the same stellar signal through a beamsplitter. This effectively removes effects of correlated afterpulsing. Except for extremely short delay times, the correlation channels affected by afterpulsing are only the first ones. To further minimize possible systematic effects, the first two channels from each measured ACO were omitted in preparing the data for Figs. 6 and 7.

### *6.6.2 Microsecond Scintillation*

Figure 6 shows scintillation on very short time scales. To make visible also small effects near the origin, the function plotted on a logarithmic scale is 1.001 minus the autocorrelation, which thus approaches 0.001 for zero time delay.

To reach very low noise levels, the data in Fig. 6 are the average of many data records, weighted according to their integration time. All data are near-zenith ($Z \simeq 20°$) summer observations of Vega at $\lambda$ 550 nm, recorded during a few adjacent nights. They comprise several sequences with sample times usually changed by factors of 10. Since most such measurements were interleaved in time, this (to first order) removes effects of atmospheric changes. The building up of a common curve was made by averaging the ACO values at each end of the delay interval, and then normalizing the successive time-lag portion accordingly, using the shape of the ACO curves for $\lambda$ 550 nm in July (Fig. 14) as a 'template' whenever the ACO had not been fully sampled over all delay times.

The data points for ∅20 cm at delays $\leqslant$10 $\mu$s are omitted, since these begin to be dominated by random photon noise. Similarly, the noisy data points for ∅60 cm at delays $\tau \leqslant$200 ns are not shown, although data were recorded down to 20-ns delay.

For longer delays (milliseconds), the general difference between the curves for ∅60 and 20 cm reflects the aperture dependence: its precise amount, however, does not reflect aperture effects only, since these data originate from different nights.

### *6.6.3 Inner Scale of Turbulence*

In the microsecond domain we could expect to find signatures of the *inner scale* $l_0$ of refractive-index fluctuations, i.e., characterizing the smallest atmospheric eddies with parameters distinctly different from their surroundings. In Fig. 6, a distinct break in the slope of the autocorrelation function can be seen for delays around 300 $\mu$s, suggesting rather different distribution functions for structures larger and smaller than the corresponding size (with rather less fluctuations in the smaller ones). The speed of the flying shadows was measured as typically $\simeq$10 m s$^{-1}$ (Paper III). At that speed, 300 $\mu$s corresponds to a linear size of 3 mm. Note that this 300 $\mu$s time scale is still three orders of magnitude slower than the most rapid scintillation component measured, and four orders of magnitude slower than our full experimental resolution.

Over horizontal paths, the inner scale $l_0$ can be determined through various scintillation methods, involving single or multiple laser beams (Hill 1992; Sasiela 1994). Typically, values of $l_0$ in the range 2–10 mm are found, apparently consistent with the value deduced here, $\simeq$3 mm. However, what Fig. 6 indicates is that the distribution function of structures in the flying-shadow patterns has a break

around 3 mm. By itself, this cannot tell from what region[s] in the atmosphere this break originates, nor what is the precise correspondence between these flying-shadow patterns, and refractive-index inhomogeneities.

Even if there is a well-defined size for the smallest significant structures in the shadow pattern, such a cutoff can be statistical only, and some structures must extend to smaller [time]scales. For delays around 10 $\mu$s, the autocorrelation function approaches unity within $\simeq 10^{-4}$, a hundred times closer than at 1 ms (Fig. 6). Whether the behavior at the shortest delays merely reflects the tail of the shadow-pattern distribution function, or whether it is also influenced by other effects is awkward to decide, due to the small magnitude of the effect, and due to the lack of previous observations showing comparable signatures.

If these deduced 3 mm do indicate a Fresnel-zone size ($\sqrt{\lambda h}$), the implied turbulence distances are $\simeq 15$ m, i.e., very close to the telescope. Under such conditions, a very good local telescope environment would be required in order to depress the most rapid scintillation components (perhaps even a vacuum solar telescope).

#### 6.6.4 *'Peculiar' Scintillation Phenomena?*

There have been occasional reports in the literature of 'peculiar' scintillation properties. Thus, Morris (1971) reported starlight being modulated at discrete radio frequencies, corresponding to those of radio stations. He suggested that their transmissions were driving electron-density fluctuations in the ionosphere, which would modulate optical starlight. Fluctuations around 1% were reported in the range 1–20 MHz. However, with very much higher sensitivity (at least in the lower MHz range), we see no hints of such modulation (despite several radio transmitters in the vicinity); we rather suspect that such frequencies entered this earlier experiment due to imperfectly shielded electronics.

### 6.7 Scintillation on 'All' Time Scales

Figure 7 merges observed autocorrelations and power spectra into a composite function, spanning more than four decades of timescale. The power spectra were obtained by transforms of autocovariance. Their jagged appearance for higher frequencies is an artifact due to numerical instabilities. The *power-density* spectrum (center) shows the density of scintillation power per unit frequency interval, while the *power-content* spectrum (bottom) shows where that power is located (mostly between 10 and 100 Hz).

These summer data originate from sequences of near-zenith ($Z \simeq 20°$) observations of Vega. By normalizing successive portions of many measurements, a common curve spanning over many time scales was obtained. The points for the shortest delays are cross correlations as in Fig. 6.

#### 6.7.1 *Windspeed Effects*

Although the total scintillation power depends on the strength of the turbulence, the *width* of the frequency spectrum depends on the speed at which the shadow pattern moves across the telescope aperture. For fixed total power, increasing the speed of motion increases the high-frequency

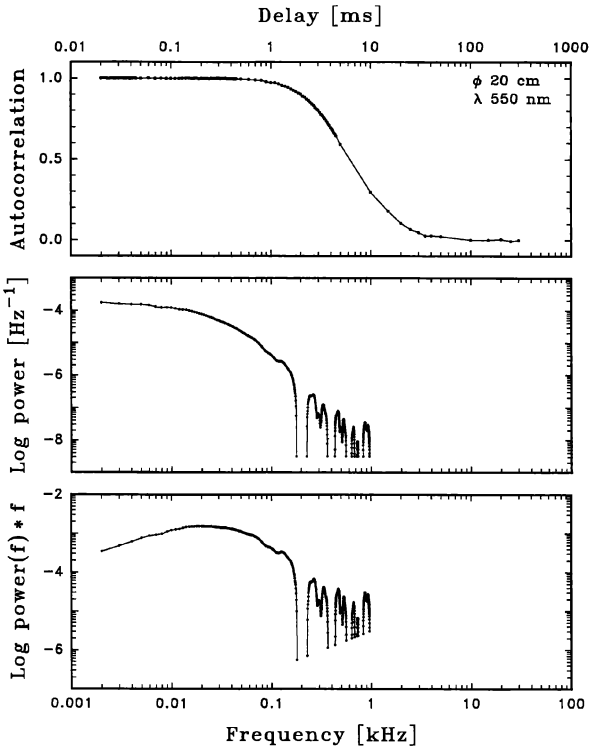


FIG. 7—Observed autocorrelation and power spectra of intensity scintillation, spanning four decades of time scale. While the most characteristic time scale of scintillation in the range of a few milliseconds, variations are detected on all time scales examined. The *power-density* spectrum (center) shows the density of scintillation power per unit frequency interval, while the *power-content* spectrum (bottom) shows that most power is located between 10 and 100 Hz. For these particular data, $\sigma_I^2 = 0.0044$.

scintillation and decreases the low-frequency one. The effects become dramatic, when comparing scintillation from the ground, with that seen from airplanes. Young (1969) evaluated measurements by Mikesell and Brown (1966) from aboard a jet airliner. The much larger effective 'wind' velocity in the aircraft (200–300 m s$^{-1}$), shifts the scintillation power to correspondingly higher frequencies, and spreads it over a much broader bandwidth.

#### 6.7.2 *Outer Scale of Turbulence*

*The outer scale* of turbulence $L_0$, is that beyond which the structure function of the wave-front fluctuations no longer increases with a standard [Kolmogorov] power law, but instead saturates. To the extent that $L_0$ is a well-defined quantity, it can be deduced from refractive-index fluctuations inferred from different classes of interferometric path length, angular or intensity scintillation measurements. Values around 10 m are often found, but sometimes ranging between a few meters to kilometers (Agabi et al. 1995; Bester et al. 1992; Buscher et al. 1995; Colavita et al. 1987; Coulman et al. 1988; Coulman and Vernin 1991; Davis et al. 1995; Nightingale and Buscher 1991). It appears that $L_0$ varies from site to site and even from night to night.

The time scale of some minutes, on which the seeing typically changes, is often referred to as 'intermittency' of

the turbulence. In a crude way, it may be associated with the outer scale. For a wind speed of 10 m $s^{-1}$, 500 s corresponds to a scale of 5 km, comparable to the plausible size of relevant atmospheric regions.

*6.7.3 'Scintillation' on its Longest Time Scales*

For *angular* seeing, power spectra have been assembled from astrometric data for time scales extending to hours, days, and even seasons of year (Høg 1968). Over the large frequency interval 10 $\mu$Hz–10 Hz, the empirical spectrum for image motion fits one single, smooth function. This could indicate that a single mechanism produces atmospheric fluctuations on scales from 10 cm to 100 km (for typical windspeeds leading to time scales between milliseconds and hours).

Perhaps, also the functions for fluctuations of stellar irradiance have a continuous extension to very long time scales? The power spectrum of scintillation proper, i.e., that component of atmospheric intensity fluctuations that originates from refractive-index variations in atmospheric turbulence, is expected to produce a flat tail at low frequencies. However, there exist many types of atmospheric oscillations and waves, which could contribute to irradiance changes. In such a case, the low-frequency tail is likely to be known under some other name, perhaps *transparency fluctuations, extinction anomalies*, or similar. Such phenomena have been studied with an aim to improve stellar (and solar) photometry.

Brightness oscillations in the daytime sky are ascribed to buoyancy or gravity waves in the atmosphere, affecting the zenith column air mass (and thus the extinction). Power spectra of such brightness oscillations are similar to those of microbarograph records, and show periodicities from a few to hundreds of minutes; the wave forms vary from day to day. Oscillations in the uppermost atmosphere are visible as variations of the airglow hydroxyl emission, and have been suggested to correlate with transparency variations.

Even on nights of apparently superb photometric quality, there are low-amplitude variations in atmospheric transparency. From stellar photometry, Clarke (1980) identified possible short-period oscillations of extinction. Their observed color dependence suggests that the waves affect the aerosol contribution some four times more than the contribution by air molecules. However, he argued that these slow changes in extinction are *not* the low-frequency part of scintillation. Power spectra for time scales of minutes were recorded by Deubner and Isserstedt (1983); Grec et al. (1977); and Schmidt-Kaler and Winkler (1984).

Vid'machenko (1994) linked brightness changes of stars (typically $\simeq$0.005 mag), observed at Mount Maidanak, with mountain lee waves, where aerosol haze forms in the wave crests. Variations in atmospheric extinction were measured simultaneously at three telescopes on Crimea by Burnashev et al. (1991), finding periods of 3–7 min.

While we cannot yet draw clear conclusions about the low-frequency tail of stellar irradiance fluctuations, it appears that there may be a continuous spectrum extending toward quite long time scales. One present limitation lies in the need for a much larger statistical sample. A 100-s integration with 1-ms resolution produces a well-defined autocorrelation for the 10-ms region, but to obtain the same number of samples for the 10-s region requires 100,000 s$\simeq$30 h. This demand on observing time accounts for the relative noise in data points for the longest delay times in Fig. 7 being much greater than for the shortest ones, precluding equally detailed conclusions. Another limitation is that, in order to average out the scintillation proper, and reveal other types of fluctuations, a large telescope is required (the scintillation observed in even 4-meter-class telescopes falls close to extrapolations from smaller apertures; Paper III).

## 7. CHANGES DURING A NIGHT

As already encountered above (e.g., Figs. 3, 5, and 10), the atmosphere undergoes various longer-term changes, affecting amplitudes and time scales of scintillation. We will now examine such changes in more detail. The value of such information lies not only in understanding the atmosphere as such, but in particular in illustrating the observational environment in searches for astrophysical variability. These systematic changes limit the maximum integration time in meaningful studies of statistical distributions (cf. Sec. 5), and determine how frequently atmospheric calibrations must be updated, to permit a certain accuracy for deducing fluctuations in astronomical sources.

### 7.1 Other Sites

The scintillation changes during and between nights can be quite profound, and the effects did not escape previous observers, some of whom documented correlations with weather patterns. Thus, Bufton and Genatt (1971) noted that two nights with well-developed jet-stream winds had scintillation extending to high frequencies ($\gtrsim$100 Hz), while one night with weaker winds was dominated by slower fluctuations ($\lesssim$50 Hz). Variability in scintillation at various observatory sites was examined by Alexeeva and Kamionko (1982) and Gladyshev et al. (1987).

Stecklum (1985) monitored $\sigma_I^2$ (white light, 1.1 cm aperture) continuously during several hours of night, finding repeated 'bursts' of scintillation, with correlation times typically between $\simeq$20 and 100 s. These results led him to suggest that the general temporal behavior of scintillation is governed by two time scales, possibly connected with those characterizing the inner and outer scales of turbulence (cf. Mariotti 1983).

### 7.2 Nights on La Palma

Figures 8 and 9 show examples of how the temporal autocovariance functions for the starlight intensity evolve throughout two consecutive winter nights. The star observed was Polaris, assuring a [nearly] constant position in the sky at zenith distance $Z\simeq60°$. The amplitude and temporal structure of scintillation is seen to evolve on time scales of typically tens of minutes.

Figure 8 shows observations with a 60 cm aperture. Data for 49 autocovariance functions are shown, each integrated for 120 s each, and sampled at 2 ms. The measurements alternated between 400, 500, 600, and 700 nm. However, the change with optical wavelength for this large 60 cm aperture

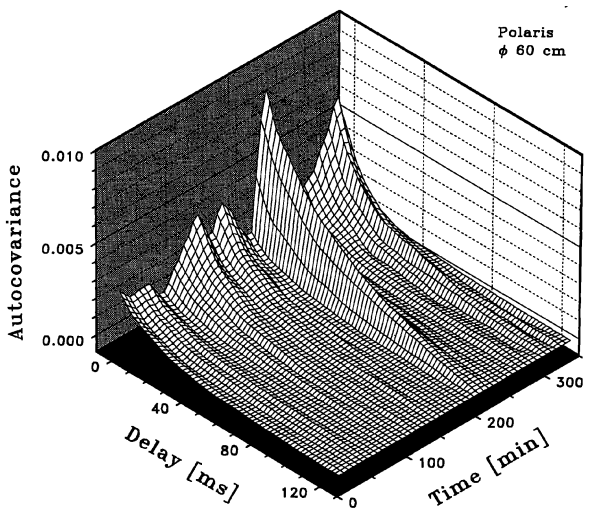


FIG. 8—The evolution of the autocovariance of stellar intensity during a night, observed through a 60-cm telescope. The star was Polaris, assuring a constant position in the sky. The amplitude at the origin equals the intensity variance $\sigma_I^2$. Each curve represents a 120-s integration. The amplitude and temporal structure of scintillation is seen to change on time scales of typically tens of minutes.

is negligible (Paper II), compared to the temporal changes, and data for the various colors are here plotted together. The amplitude of each autocovariance at the origin equals $\sigma_I^2$. That was computed from probability distributions, which were measured alternately with the autocorrelations, here interpolated to the precise epochs of the latter recordings. The beginning of that night featured a stable stellar image, with only slow image motion visible. The final third, or so, of the measurements showed some evidence of drifting thin clouds. The [ground] wind was weak throughout the night.

*Two* time scales are obvious in Fig. 8: that given by the autocovariance half-width, which [for the 60 cm aperture] is about 15 ms, and one around tens of minutes, characterizing the evolution of amplitude and temporal structure. This is not unlike the 'bursts' of scintillation seen by Stecklum (1985). Also, site testing at various observatories often shows the atmospheric water vapor content to change on such scales of tens of minutes, even on photometrically excellent nights.

A closer examination of Fig. 8 reveals how variable scintillation can be. The large burst in amplitude at ≃220 min is accompanied by a big increase in time scale, possibly suggesting a sudden incursion of low-level, low-speed turbulence. In contrast, the burst of scintillation at ≃330 min is *not* accompanied by any such change in time scale. That, apparently, was just a patch of upper-level turbulence advected along by the wind in the upper troposphere.

Figure 9 shows the evolution (on the following night) of the spatially smaller patterns of higher contrast, as sampled through a small 9 cm aperture. Note that both the vertical and horizontal scales now differ by one order of magnitude from those in Fig. 8. These more rapid fluctuations were measured with a sample time of 400 $\mu$s, again integrating 120 s for each record. A 50 min intermission in observations at the middle of the night appears as an empty space, with 33 records before this break, and 22 after it. These measurements were intermingled with such for probability distributions, from which the $\sigma_I^2$ values used for normalizing the autocovariances originate. The small entrance aperture made the speckle image of Polaris almost invisible on the TV monitor, and we thus have no real data on the image properties.

Also here, measurements were made at different wavelengths. As expected for a smaller aperture, $\sigma_I^2$ now slightly varies among different colors (Paper II), although these differences are not greater than the measurement noise in individual records, and rather smaller than the temporal changes. Therefore, no segregation between measurements in different colors was made for Fig. 9.

In our observations, a fixed telescope senses the moving atmosphere above. Somewhat equivalent measurements can be obtained with a telescope rapidly moving through the atmosphere. Such experiments, with two airplanes flying in formation (a light source on one, observed from another) have been made for separations around 50 km, at altitudes spanning the tropopause (Stroud 1996). Significantly different scintillation was observed after flying 5–10 km, not unlike our scales on tens of minutes, which (for winds of ≃10 m s$^{-1}$) do correspond to such distances.

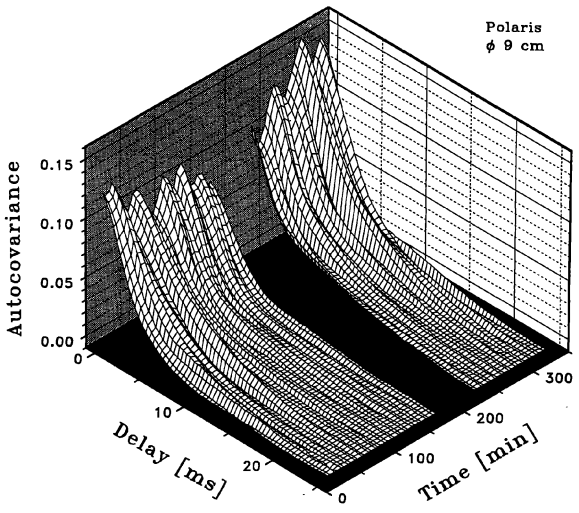


FIG. 9—The evolution of the autocovariance of stellar intensity during another night, measured through a small aperture of 9 cm. This samples the spatially smaller scintillation patterns of higher contrast: both the vertical and horizontal scales differ by an order of magnitude from those in Fig. 8.

## 8. ZENITH-DISTANCE DEPENDENCE

Scintillation varies with position in the sky. The strongest dependence is that with zenith distance, which is examined in this section.

### 8.1 Observational Background

Stars near the horizon scintillate with greater amplitude but more slowly than stars near zenith: this causes the [low-frequency] naked-eye twinkling to become prominent near the horizon. This zenith distance dependence has been measured by Bufton and Genatt (1971); Darchiya (1966); Diamant et al. (1969); Ellison and Seddon (1952); Fuentes et al.

(1987); Gladyshev et al. (1987); Knoechel and von der Heide (1978); Mikesell (1955); Mikesell et al. (1951); Parry et al. (1979); Protheroe (1955a); Siedentopf and Elsässer (1954); Stecklum (1985); Zhukova (1958), and others.

Although the scintillation increases away from zenith, the increase does not continue until the very horizon. Typically, the amplitude increases until around $Z \simeq 60°$ or perhaps 70°, whereupon it saturates (or even decreases). The saturation angle depends on the airmass traversed, and may differ between low- and high-altitude sites: in data from Pamir at 3,860 m altitude, there was no evidence for saturation even at zenith distances $Z \simeq 80°$ (Darchiya 1966). Only a few studies at extreme zenith distances seem to exist, e.g., Butler (1952) who recorded scintillation at an elevation of only 1° above the horizon.

More subtle effects include the aperture-size dependence for the saturation angle, being closer to zenith for smaller telescope apertures. Further, the validity of a log-normal distribution seems to become weaker with increasing zenith distance (Stecklum 1985).

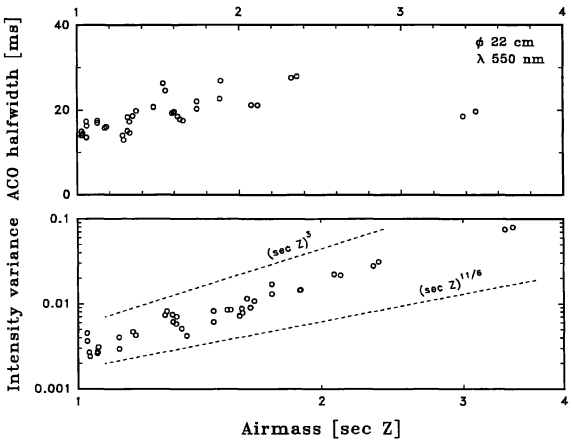


FIG. 10—Scintillation amplitudes and time scales increase with zenith distance, here measured with a 22 cm aperture at largely constant azimuth angle. Top: For moderate airmasses, the autocorrelation halfwidths increase roughly as sec Z, as expected from geometrical effects (but the effect is not striking, and does not extend to the largest airmasses). Bottom: the increase of $\sigma_I^2$ with sec Z, and the theoretical slopes for large (3), and small apertures (11/6).

### 8.2 Theory

Theories have been developed in the wave-optical treatment by Tatarski (1961), and in the geometrical optics one by Reiger (1963). Although different in other aspects, these agree on the zenith angle dependence, $(\sec Z)^3$, for large apertures. The concepts are discussed by Bufton (1973) and Parry et al. (1979). Equations (3) and (4) predict for the wave-optics case (small apertures) a dependence $\sigma_I^2 \propto (\sec Z)^{11/6}$, and in the geometrical optics case (large apertures) $\sigma_I^2 \propto (\sec Z)^3$.

To account for saturation at large zenith angles, Young (1969; 1970a, b) showed how effects of [angular] seeing and color dispersion cause deviations from this $(\sec Z)^3$ dependence: light traversing large airmasses is spread out laterally, thus providing spatial averaging. The zenith-distance dependence of the scintillation index $\sigma_I^2$ can be numerically modeled under certain assumptions. The results show how $\sigma_I^2$ increases until some zenith angle, then saturates and finally decreases near the horizon (Beran and Whitman 1988).

### 8.3 Azimuth Effects

Away from zenith, also the azimuth angle of the star in the sky becomes a significant variable. Since scintillation depends on the speed of the flying-shadow pattern, geometrical projection effects for the azimuth angle of the wind velocity may cause changes in time scale of equal importance as those due to a changing zenith angle (Young 1969). When looking away from the zenith, the projected windspeed perpendicular to the line of sight $V_\perp$, in general is smaller than the actual value $V_0$ (assuming horizontal winds). When looking directly into, or away from the wind, $V_\perp = V_0 \cos Z$. Temporal phenomena scale with these factors.

In the literature, there seem to exist only very few measurements of how scintillation power spectra change with the wind azimuth (Filippov 1972). Since it is impossible in practice to simultaneously observe the dependence on every parameter, some authors have avoided interference from azimuth effects by selecting stars near one azimuth only (Stecklum 1985).

In passing, we note that *naked-eye* twinkling of stars does *not* depend on azimuth. The reason is more subtle: For the relevant small-scale fluctuations near the observer, the wind-shear translates the power spectrum nearly parallel to itself, not changing the low frequencies seen by the eye (Young 1969).

In the present work, only a limited effort was put into studying the dependence on Z. One reason was that any significant improvement over previous studies demands [quasi]simultaneous observations over many azimuths and zenith distances, something that was beyond our resources. Another reason is that, in searches for astrophysical variability, one will observe near zenith whenever possible, to minimize atmospheric effects.

In our data, the dependence on azimuth was limited by choosing stars in the southern part of the sky. Since the predominant wind direction on La Palma is from the north, this means that most measurements were roughly in directions away from the wind.

### 8.4 La Palma Results

Figures 10 and 11 show our results for the zenith-distance dependence for scintillation amplitudes and time scales. Both amplitudes and characteristic time scales increase with Z. The increasing autocorrelation halfwidths (13 to 27 ms) may be interpreted as a geometrical projection effect, at least for moderate zenith angles. Along the wind azimuth, the time for a disturbance to traverse the aperture increases as sec Z. This roughly seems to happen, although the effect is not striking, and (due to effects of wind azimuth or perhaps incipient saturation?) does not extend to the largest airmasses. More

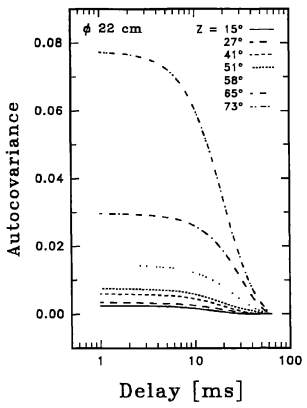


FIG. 11—Representative autocovariance functions are shown at about 10° intervals in zenith angle, measured with a 22 cm aperture at roughly the same azimuth. There is a dramatic increase of scintillation amplitude for larger Z.

precise data could permit analyses versus not merely sec $Z$, but also against some turbulence-airmass factor, computed from vertical profiles of $C_n^2(h)$.

The bottom panel in Fig. 10 shows the increase of $\sigma_I^2$ with sec $Z$, and the theoretical slopes for large–$(\sec Z)^3$, and small apertures–$(\sec Z)^{11/6}$. We find an essentially linear relationship between $\log(\sigma_I^2)$ and $\log(\sec Z)$ with slope $\simeq 2.7$, in rather close agreement with the theoretical value of 3, although the 22 cm aperture here cannot be much larger than the Fresnel-zone size $r_F$. Corresponding power spectra (not plotted) show that only fluctuations $\lesssim 30$ Hz are significantly affected.

These data originate from measurement sequences, rapidly alternating between probability distribution functions and autocorrelations, for ten different stars during one winter night. The curves in Fig. 11 are averages from pairs of measurements, yielding one curve per star. Mechanical limitations of the telescope precluded observations very near the horizon.

## 9. ANGULAR COHERENCE AND BINARY STARS

The previous chapter treated scintillation changes along large angles across the sky. We now examine the finer-scale angular dependence: over how large an angle can scintillation be considered constant?

The exact dependence on angular extent can be rather complicated. The light from two very nearby stars traverses the same atmospheric inhomogeneities, and 'must' show the same statistics of scintillation. Stars near zenith, a small angle $\Theta$ apart, cast on the ground similar shadow patterns, shifted horizontally by a distance $\Theta h$, where $h$ is the height of the relevant turbulence layer. Even with identical shadow patterns, such shifts may cause a temporal 'phasing' relationship between the components of a binary star (that further depends on their position angle relative to the wind azimuth). As a result, for larger sources (as for planets), the flying shadows lose their sharpness. Compared to a single star, the scintillation from a binary or a planet may differ in amplitude, in power spectrum, and also in the dependence on, e.g., zenith distance or telescope aperture.

### 9.1 Previous Observations of Binary Stars

Binary-star components may undergo *coherent* image motion, while their scintillations are *incoherent* (i.e., the averaged irradiance from both components scintillates less than each of them; e.g., Hosfeld 1954). Possibly, such effects can be explained by lateral shifts of the shadow patterns.

One of the binaries studied by Protheroe (1955a) with a 32-cm telescope had sufficient separation ($\rho$=22 arcsec) to permit each component to be measured individually as well as in combination. The data indicate some sort of 'phasing' relationship between the signals from the component stars (the combined signal fell below that expected for 'random' combination). For a closer binary ($\rho$=2.5 arcsec), the aperture dependence was found to differ from that for a single star. Campbell and Elford (1990) found the intensity variance of a binary ($\rho$=4.3 arcsec) to be less than for a single star (measured in very small telescope apertures), consistent with the scintillation of each component being almost uncorrelated. Various shadow correlations in binary-star scintillation were exploited by Rocca et al. (1974) to infer properties of atmospheric turbulence.

### 9.2 Planetary and Solar Scintillation

The scintillation power of planets is distinctly lower than for stars (Ellison and Seddon 1952; Filippov 1972; Protheroe 1955a; Young 1969). For Jupiter ($\simeq$35 arcsec disk), the attenuation around 10 Hz reaches some two orders of magnitude. The power spectrum differs, in that there is a relative lack of high frequencies. The effects are more pronounced in small apertures, although the dependence on aperture size seems less significant than for stars (Akimov et al. 1992). When the diameter of a planet falls below some 3 arcsec, its scintillation approaches that of a star; e.g. [within the accuracies of past measurements] the main Jupiter satellites (1–2 arcsec) scintillate almost like stars.

The *Sun* (diameter $\simeq$30 arcmin) is much greater in angular extent than any planet, and its scintillation is very much smaller, though still measurable (Wessely and Mitchell 1971). The probability distribution of the irradiance is now accurately described by a Gaussian function (because the tiny scintillation amplitude makes this impossible to distinguish from a log-normal one). The dependence on angular extent can be followed as the solar disk gradually becomes occulted during a partial eclipse (Georgobiani et al. 1995).

Grec et al. (1977) found atmospheric transparency fluctuations to be highly correlated over scales of arcminutes. Whereas scintillation can be reduced by increasing the telescope aperture, they found no evidence that transparency variations could be significantly reduced by such means.

The question of coherence over larger angles was addressed by Zwicky (see Oosterhoff 1957), who noted that scintillation effects of aerial 'blobs' and 'eddies' sometimes remain over several arcminutes. Compression waves caused by jet planes, lightning, and bullets could be followed practically over the whole sky.

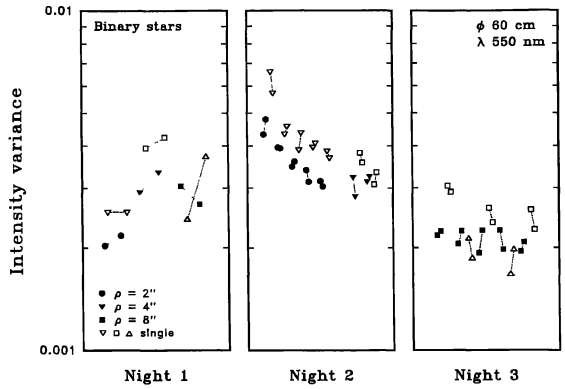


FIG. 12—Intensity variance for binary stars with equally bright components, but with the successively greater separations of 2, 4, and 8 arcsec, compared to single stars. The variance is systematically smaller for binaries, showing that the scintillation patterns are perceptibly different already some arcseconds away in the sky.

### 9.3 Theory for Extended Sources

In developing a theory for planetary scintillation, Young (1969) identified a *planetary-filter* function analogous to the aperture one, but containing also the atmospheric height. With increasing height, this function increasingly filters out the high spatial frequencies of refractive-index variations. For *very* extended sources (such as the Sun), the contribution functions to angular seeing and to intensity scintillation tend to become similar. This can be exploited in site testing, searching for the best *angular* seeing, without any need for a telescope (Beckers 1993; Seykora 1993).

Because no planet presents a uniform disk, the detailed interpretations are more subtle. Jupiter is limb-darkened, which effectively apodizes the planetary filter function, reducing the high-frequency components. The rings of Saturn both introduce more high frequencies (because of their sharpness) and reduce low ones (because their extent is greater than the planet's; Young 1969). Theoretical aspects for sources of finite extent are also discussed by Sasiela (1994).

### 9.4 Present Observations of Binary Stars

For the present program, different binary stars (within the same focal-plane aperture) were observed. Probability distributions and autocorrelations were measured during a few hours in each of three summer nights, and compared to those of nearby single stars. These measurements were with the 60 cm aperture and a λ 550 nm filter, at typical zenith distances ≃30°; Fig. 12.

Binaries were selected to have separations increasing in geometric progression (≃2, 4, and 8 arcsec), and to have equally bright components. For calibration, nearby single stars were measured alternately. These stars were: ζ Aqr (component magnitudes $m_v$=4.4 & 4.6), whose separation at the epoch of observation was measured on a speckle-image TV monitor at the telescope to ≃1.″8 (catalog value at some unspecified epoch=2.″0), with γ Aqr as its standard. For 65 Psc ($m_v$=6.3 & 6.3), the separation was estimated as ≃4.″4 (=catalog value). The visual impression gained from the real-time TV monitor was that the speckle patterns for the [well-resolved] components of 65 Psc were quite similar. Its standard star was 67 Psc. For the largest separation, γ Ari ($m_v$=4.8 & 4.8) was used (measured ≃8.″4, close to its catalog value of 8.″2). Two different standard stars were used here (one slightly lower, another higher in the sky): α Tri and *o* Psc.

As seen in Fig. 12, the measured variance is systematically 10%–20% smaller for all binary stars, demonstrating that the scintillation patterns are perceptibly different [and/or displaced] already a few arcseconds away in the sky. Figure 12 also indicates the need for near-simultaneous measurements of binary and standard stars, lest the effects become masked by intrinsic temporal changes in the atmosphere (cf. especially the center panel).

The 'full' segregation of effects between single and binary stars would require small telescope apertures (5 cm, say). Two arcsec is $10^{-5}$ rad; at 10 km altitude, the ray separation is only 10 cm; and 40 cm for 8 arcsec—still smaller than the aperture used here. Thus, although the rays from the stellar components largely sample the same column of air, Fig. 12 illustrates that effects are still visible even at such 'large' apertures.

Also autocorrelation functions (not shown) reveal differences between binary and single stars. Binaries scintillate somewhat slower (autocorrelation half-widths are ≃20% longer), apparently because the most rapid fluctuations are averaged out more, analogous to spatial averaging in larger telescope apertures.

With our measuring precision, effects could be expected to be visible also in comparing single stars with Jupiter's satellites. Unfortunately, attempted observations did not give good data because Jupiter happened to be low in a part of the sky where the telescope tracking was unstable.

## 10. CORRELATION WITH ANGULAR SEEING

Links between intensity scintillation and angular seeing have been sought in vain by many investigators, leading to the conclusion that the correlation is very weak, if any. This can be understood theoretically (e.g., Roddier 1981, his Chap. 8), because the contribution function for angular seeing is weighted toward the lower regions of the atmosphere (in particular those near the ground), while that for scintillation singles out high layers. Since, at 'regular' observatory sites, the contributions from upper and lower atmospheric layers are of comparable magnitude, (e.g., Roddier and Vernin 1977), one is not likely to find distinct correlations between variability in such separated atmospheric regions.

### 10.1 Possible Mechanisms

However, while such a lack of correlation may be valid at most 'ordinary' sites, from where such studies were made in the past, the situation could be different for premier astronomical observatories at the best locations. Some of these were selected in recent decades following extensive micrometeorological site surveys (e.g., La Palma, Mauna Kea, Paranal). A common property of these is that their local topography enforces a smooth and laminar airflow of nearly

isothermal ocean air across an aerodynamically shaped mountain where the observatory is situated. Man-made turbulence at ground level is minimized through careful design and siting of buildings in the landscape, diverting their heat emissions to downwind areas. As a result, the ground-level contribution to angular seeing is greatly reduced. The quality of the subarcsecond seeing that is regularly experienced is now set by the high-altitude turbulence, the *same* layers that produce scintillation. Under such conditions, we could actually expect some correlation between seeing and scintillation.

What correlation to expect is not obvious. Naively, less turbulence must ultimately (in free space) lead to diffraction-limited images without scintillation, i.e., then a decrease of scintillation should correlate with smaller images. However, in a turbulent atmosphere, one could also encounter the *opposite* correlation since, at least in principle, an increase in angular spread decreases the scintillation by averaging over a larger column in the atmosphere. From high in the atmosphere, any small telescope aperture subtends an angle of not many arcseconds, so seeing can produce some smearing and thus effective enlargement of this aperture, as seen from those layers that produce the scintillation. Each star can then be regarded as a small disk of perhaps 0.2 arcsec extent. This is *not* the seeing disk seen by an observer looking up from the ground, but rather that which would be seen looking *down* through the atmosphere. At 'ordinary' sites, this seeing disk will be much smaller than the angular seeing looking up, because of the concentration of the turbulence toward the bottom of the atmosphere. For good sites, however, this difference will be rather less. On the other hand, e.g., a 60 cm aperture (Fig. 13 below), subtends $\simeq$10 arcsec as seen from the upper atmosphere, and any differential smearing caused by changes in such subarcsecond seeing would appear to be negligible.

### 10.2 Naked-Eye Twinkling

The well-known correlation between naked-eye twinkling and poor seeing is understandable since twinkling ordinarily originates from Fresnel-zone sized features in the near-surface boundary-layer turbulence, the region chiefly responsible for bad seeing at 'ordinary' sites (Young 1969; Warner 1988). At premier observatories such as La Palma, the visual twinkling of stars is almost imperceptible during good summer conditions, and barely visible in winter: for any visitor this is a most striking difference compared to 'ordinary' locations.

### 10.3 Previous Studies of Seeing-Scintillation Relations

A most convincing demonstration of the lack of correlation between local turbulence and scintillation was reported by Hosfeld (1954) and Protheroe (1955a). Warm air was suddenly introduced into a cool telescope dome at night. As a result, the star images were set in violent agitation, without any perceptible effect on the simultaneously measured scintillation. The same authors also studied the *daytime* scintillation of stars. Although the increased ground heating during daytime normally generates a poor angular seeing, scintillation is only marginally different from its nighttime values.

Although he generally found but little correlation, Mikesell (1955) noted several cases when small scintillation was observed simultaneously with very bad seeing. Protheroe (1955a) noted cases of the opposite.

### 10.4 Seeing Correlations on La Palma

In a first search for a possible correlation, we used seeing data from the Carlsberg Meridian Circle. This automatic telescope, located nearby (a few hundred meters) at the observatory, measures stars along the north-south meridian. Its data products include seeing disk sizes at different elevations, and at different times of night. These do well illustrate changes in weather and seeing patterns, and were compared with our scintillation data for some ten nights. However, no sensible correlations could be identified. The explanation could be the generally expected lack of correlation, but perhaps also that this telescope is too small (∅ 18 cm) to really distinguish between very good and excellent seeing.

### 10.5 Speckle-Image Correlations

A more elaborate search for possible correlations between scintillation and image properties was made by making a continuous video recording of the stellar speckle images, simultaneously with scintillation measurements in the same 60 cm aperture. A beamsplitter sent some of the light through a microscope objective, focusing a greatly enlarged stellar image onto an image-intensified video camera, connected to a tape recorder, running at 50 [half]frames per second. The other part of the light went to the photomultiplier for our regular measurements. The star was again Polaris, assuring no changes in airmass nor azimuth (although azimuth effects could still enter from a possibly changing wind direction); Fig. 13.

The hours of video sequences were first examined by watching the speckle movie on television, and making notes about successive changes in seeing (of course without any recourse to the scintillation measurements, whose results at the time were unknown to the image examiner). Next, the video was examined through a 'frame-grabber' and image digitizer unit, connected to a computer. The stellar speckle patterns can sometimes change quite drastically from one video frame to the next. Using the 'frame-grabber,' the video image was frozen every few seconds or so, to give samples of its instantaneous appearance. Such an examination gives a feeling as to which types of image were typical at each epoch. Then, a representative image was chosen inside a 10-s time window, once every minute of time, producing a sequence of one representative speckle image per minute of time. This procedure is necessarily somewhat subjective but, after spending days in front of the monitor, the image examiner felt that it gave a reasonably accurate representation of at least the gross changes in seeing patterns. Analogous to the trends seen in Figs. 8 and 9, such changes often occur on time scales of tens of minutes.

The data in Fig. 13 originate from a winter night; the wind was weak, from south/southwest (not the most common di-

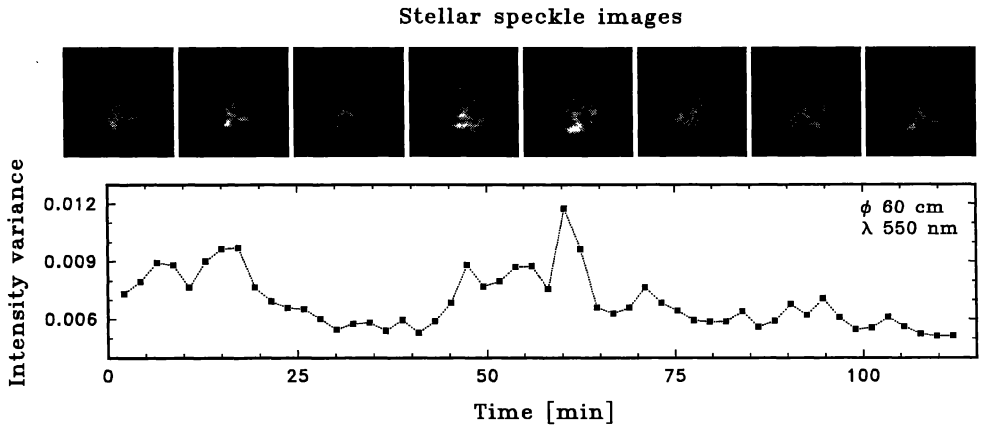


FIG. 13—The correlation between intensity variance and appearance of stellar speckle images, the latter a measure of the angular seeing. The starlight passed a beamsplitter, and a continuous video recording of a greatly enlarged stellar image was made simultaneously with intensity measurements. The star was Polaris, at a constant position in the sky. Representative stellar images are shown at different epochs along the time axis. There appears to be a correlation, such that moments of good angular seeing correlate with moments of high intensity variance, while periods of poor seeing are accompanied by lower variance.

rection). For best sensitivity in the TV camera, the video was recorded through a λ 600 nm filter, while scintillation was measured at λ 550 nm. The angular extent of each bright speckle is that corresponding to diffraction in the 60 cm aperture (≃0.3 arcsec). The wings of the stellar image here extend over several arcseconds. That is *not* representative for the seeing quality, but was rather caused by some optical misalignments in the setup for this experiment. Changes in angular seeing do not affect this instrumentally induced 'halo,' but rather reveal themselves as changes in the core of the image, where the number and contrast of speckles varies in response to atmospheric changes.

### 10.6 Discussion

Figure 13 shows the intensity variance on a common time axis with representative images from the speckle-image sequence, recorded at epochs corresponding to the placement of the image centers along the time axis. A comparison between the full image sequence (as well as the selection shown here) with intensity variance, *does suggest a correlation*, such that moments of good [angular] seeing correlate with moments of high intensity variance, while periods of poor seeing are accompanied by low variance.

Another type of measurement, characterizing moments of good angular seeing and large intensity variance was already illustrated in Fig. 5: also at that particular occasion, good seeing was accompanied by a larger contrast in the flying shadows (as shown by a greater amplitude of scintillation), as well as a greater lifetime of their features (as indicated by anticorrelation dips in the autocovariance).

When starting these analyses, we did not really expect to find much of a correlation. A few plausible mechanisms were raised in Sec. 10.1, but we must concede that our understanding of these correlations is incomplete. Increased turbulence causes a competition between both an increase of scintillation due to greater refractive-index fluctuations, and a [slight?] decrease of it through more spatial averaging due to angular smearing, and with several secondary effects likely to enter. There appear to be no previous comparable observations with which to compare our results.

In order to repeat such an experiment, a number of improvements would be useful. For example, our time resolution between video frames of 20 ms was often insufficient to resolve motions in the speckle pattern (probably requiring ≲5 ms). If the speckle movie had been digital, more quantitative measures of image parameters had been possible. The measurements were of Polaris at its rather large zenith distance of ≃60°. On one hand, the somewhat greater variability in seeing away from zenith could have made these correlations more visible, but a theoretical modeling of the phenomenon would be easier if possible zenith-distance effects could be excluded. And, not least, a rather larger telescope (∅≳2 m) is needed to match the intrinsic seeing quality at the best sites.

## 11. DIFFERENT APERTURES, COLORS, AND SEASONS

In this final observational section, we amalgamate the scintillation properties on La Palma in terms of their overall dependence upon telescope diameter, optical wavelength, and season of year. The merging of many representative measurements into Figs. 14–16 will show which trends remain over, e.g., different seasons of year, and which do not.

The parameter causing the greatest dependence (aperture size) is shown in parallel with that giving the second strongest (wavelength), illustrating, e.g., how the wavelength dependence vanishes in the largest telescope apertures. Measurements during different times of year indicate the typical difference between excellent summer conditions ('July') and normal winter weather ('November').

### 11.1 Observations

The summer ('July') data are observations of Vega at zenith distances between ≃10° and 40°. The switching between different-sized apertures was made in rapid succession, and in an intermingled order (20–2.5–10–1.2–5–20

cm, etc.). The λ 400 nm data are averages of four cycles over these apertures (each with autocorrelations measured with sample times of both 100 μs and 1 ms). The data for 550 nm are the average of seven such cycles, and 700 nm of eight. An equally rapid switching to the large 60 cm aperture was not possible, which was measured a few times between the cycles for smaller apertures. The measurements for λ 550 nm originate from one night, and those for 400 and 700 nm from another.

The winter ('November') measurements are of Polaris at $Z \simeq 60°$; for each aperture five pairs of autocorrelation measurements ($\Delta t = 400$ μs and 2 ms), were made during one night. These measurements were interspersed with those of probability distribution functions.

The apertures used in winter and in summer were not identical. The very smallest ones were used only in summer: their lower photon flux causes these curves to be somewhat noisy (e.g. ∅1.2 cm at λ 700 nm gave a count rate of only ≃300 Hz).

### 11.2 Rationale

Despite the often dramatic changes in amplitudes and time scales (e.g., Figs. 5, 8, and 9), the statistical relations between different functional dependences seem to remain conserved. There appear to be no observational nor theoretical indications that the functional dependences on telescope aperture size or optical wavelength would *themselves* depend on, e.g., the amplitude or time scale of scintillation (at least until saturation is reached). Therefore, it is possible to display such dependences in one single plot, provided the various measurement series are carefully normalized to the same atmospheric conditions (however, a straight plot of the 'raw' measurements shows a large scatter due to temporal changes in the atmosphere, which largely obliterates other dependences).

### 11.3 Data Processing

The winter data displayed here are only for one wavelength and from one night. Since these measurements were accompanied by independent determinations of the variance, the autocovariances could be directly normalized to these values. (Actually, the values for 'λ 550 nm' in Fig. 15 are the geometrical means of [the very similar values of] measurements made at 500 and 600 nm.)

The steps in the data normalization included the following:

(a) Merging of ACO curves for short and long sample times, forcing them to overlap in the regions of smallest gradient.

(b) Normalizing ACOs at short delays to 1, and ACVs to $\sigma_I^2$.

(c) To enforce a correct wavelength dependence, all variances for the aperture sequence of ACVs at each wavelength were multiplicatively normalized, such that the 2.5 cm aperture obtained that value of $\sigma_I^2$, which was measured during a special sequence with the 2.5 cm aperture only, involving rapid switching between 400, 550, and 700 nm.

(d) All variances were next normalized to the constant zenith distance $Z = 45°$, assuming a dependence of $\sigma_I^2 \propto (\sec Z)^3$, following standard models [Eq. (4) in Sec. 4]. This makes the winter ($Z \simeq 60°$) and summer ($Z \simeq 10°$–$40°$) data directly comparable, and also takes out zenith-distance effects during and between nights. In zenith, the intensity variance $\sigma_I^2$ is ≃35% of its value at $Z = 45°$.

A normalization to $Z = 45°$ was thus made for the scintillation *amplitudes*. However, no manipulation was attempted for the *time scale* (cf. Fig. 11). At larger zenith distances, the distance to the atmospheric regions causing scintillation increases, making the spatial Fresnel zone, and the time scales larger. Perhaps such a scaling could have been feasible, but it would have introduced new uncertainties, e.g., the $Z$-dependence is steeper for small apertures than for large ones. In the former case, one can expect the half-width to be proportional to the airmass, i.e., to sec $Z$. For ∅20 cm, we empirically found the halfwidth to approximately scale as $(\sec Z)^{0.8}$. Without any correction applied, some of the differences between the summer and winter curve *shapes* could reflect effects of different $\langle Z \rangle$.

(e) A remaining inaccuracy in $\sigma_I^2$ appears to originate from nonlinear changes induced by the atmosphere over time scales of only minutes, over which we must average or interpolate. For optimum parameter estimation, a global fit was made to the [logarithmic] $\sigma_I^2$ values for the joint dependence on aperture and wavelength. The program finds that matrix, $\sigma_I^2(\varnothing_i, \lambda_j)$, which [in the least-squares sense] best reproduces observed *ratios* between the variances for different apertures and wavelengths, while tolerating any absolute levels of $\sigma_I^2$. For numerical stability, the λ dependence was constrained to be monotonic with ∅ (but without restrictions on sign or magnitude). Solutions for the summer and winter data gave stable results for all apertures except 60 cm. This has only a quite small amplitude of scintillation, and no color dependence could be identified. The variances for ∅60 cm were therefore taken as the geometric mean of its different measurements. The output from this final data manipulation is believed to reveal the most credible combination of aperture and wavelength dependence, and these are the data in Figs. 14–16.

### 11.4 Autocorrelation

Figure 14 shows autocorrelation functions for different apertures, colors, and seasons. Again, the time scale of scintillation decreases with decreasing aperture size until ∅≲5 cm, when the structures in the 'flying shadows' on the ground appear to become resolved: the autocorrelation halfwidths (as well as the fluctuation amplitudes seen in Figs. 3 and 15) then become largely independent of aperture size. There is a slight continued decrease in time scale in going down from 5 to 2.5 to 1.2 cm, indicating some non-negligible contribution from also such small spatial structures. On these scales, also differences between different colors become apparent (the fluctuations become slower for longer wavelengths; Paper II).

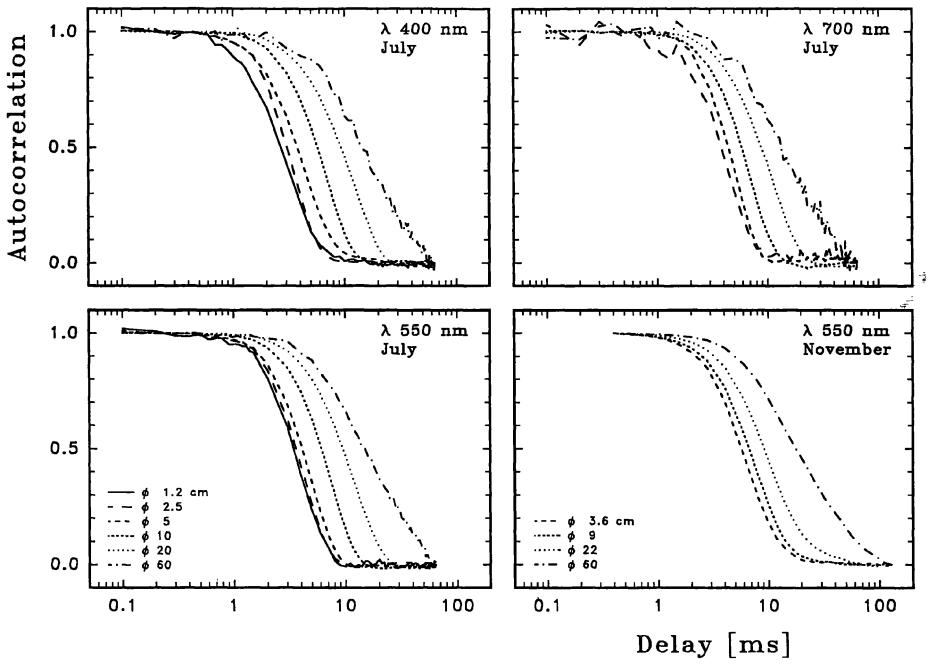


FIG. 14—Representative data for intensity autocorrelation for different apertures, colors, and seasons. The parameter causing the strongest dependence (aperture size) is shown in parallel with that for the second strongest (wavelength). The wavelength dependence vanishes in the largest apertures. Typical differences between excellent summer conditions ('July') and winter weather ('November') is shown for one color. The time scale of scintillation decreases with decreasing aperture size until $\varnothing \leq 5$ cm, when the structures in the 'flying shadows' on the ground become resolved. On these small spatial scales, also differences between different colors become visible: scintillation is slower at longer wavelengths.

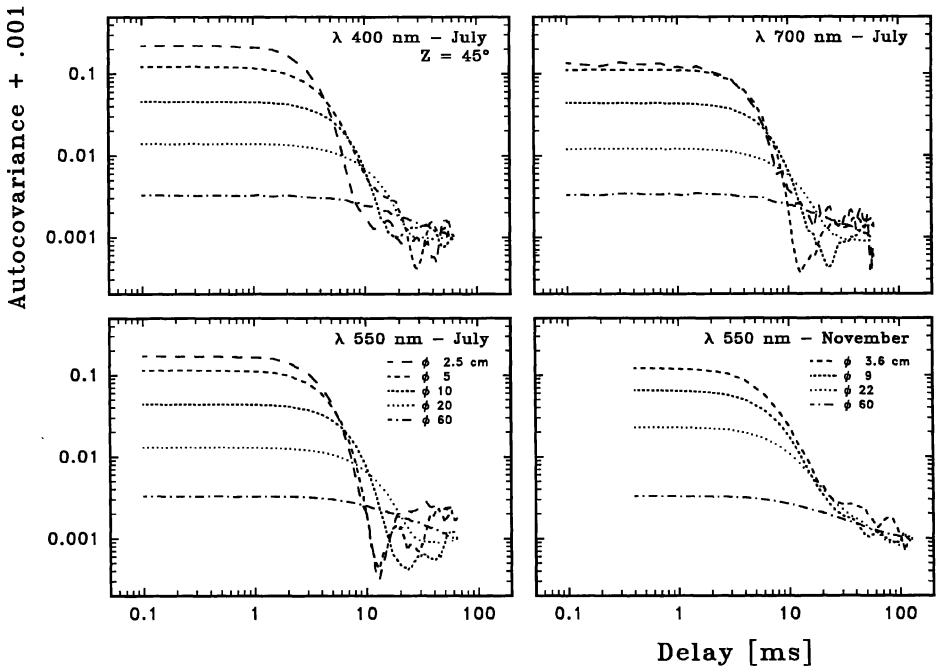


FIG. 15—Intensity autocovariance for different apertures, colors, and seasons. To view also the fine details near the zero level, the quantity logarithmically plotted is the autocovariance *plus* 0.001. During good summer conditions ('July') the 'flying shadows' are sufficiently regular and long-lived to generate *anti-correlation dips* in the autocovariance functions for the smallest apertures. This is absent in winter ('November'), probably because the structures are then smeared out by wind shear. All amplitudes are scaled to $Z=45°$, using a standard relation for the zenith-distance dependence. In smaller apertures, color effects become visible: scintillation amplitude is greater in the blue, than in the red.

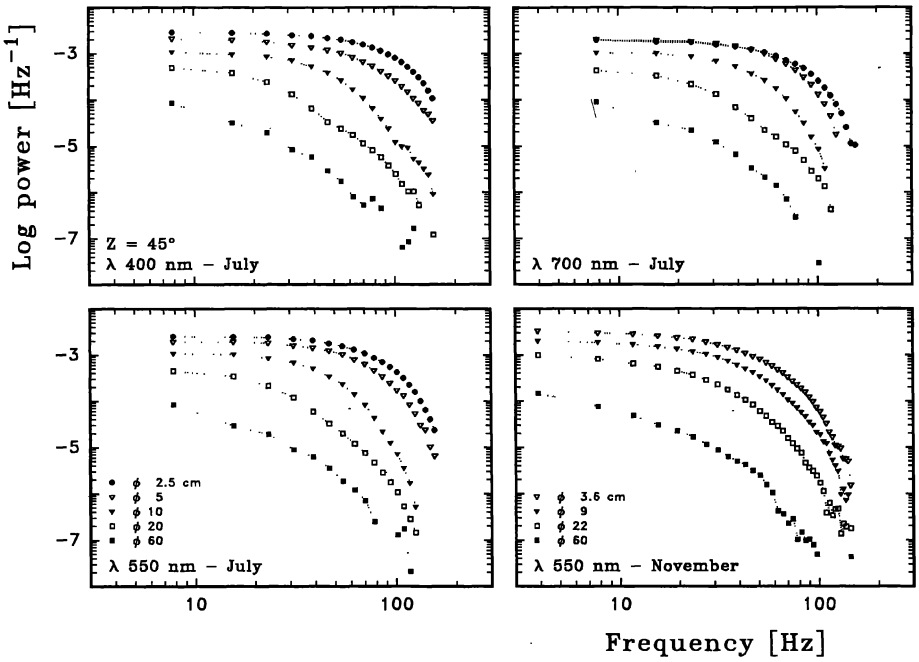


FIG. 16—Power spectral densities of intensity scintillation for different apertures, colors, and seasons. The power increases with decreasing aperture size until $\varnothing \lesssim 5$ cm. For larger apertures the power decreases (especially at high frequencies, i.e., scintillation becomes 'slower'), reflecting the spatial averaging of small-scale elements in the shadow pattern. The power spectra were obtained by directly transforming autocovariances, producing a number of discrete data points.

### 11.5 Autocovariance

Figure 15 shows intensity autocovariance for different apertures, colors, and seasons. To reveal also the fine structure near the zero level, the quantity logarithmically plotted is the autocovariance +0.001 (some ACVs become slightly negative, and this number was added to enable a logarithmic plot format).

During good summer conditions (July), the 'flying shadows' are sufficiently regular and long-lived to generate distinct *anticorrelation dips* in the autocovariance functions for the smallest apertures, at delays around 10–20 ms. The shadow pattern has alternating brighter and darker patches; that an anticorrelation remains visible after averaging over several minutes ($10^4$–$10^5$ scintillation time scales) indicates a constancy of windspeed over such periods. Such anticorrelations were never observed in the winter season (not even for stars close to zenith), probably because the structures were then washed out due to wind shear or more complex wind systems.

Atmospheric turbulence, of course, does not add nor subtract photons: it merely displaces them. To balance the region of positive correlation near zero displacement, there will in general be compensating regions of negative correlation at larger displacements in the two-dimensional shadow pattern. This information is preserved in the mapping of the two-dimensional spatial pattern to the one-dimensional temporal autocovariance only if there is a well-defined wind-velocity vector. Collapsing the 2-D pattern to 1-D already causes smearing to some extent, while wind shear or multiple wind components smear the patterns even more, as seems to be typical for La Palma winter conditions.

Perhaps the cleanest 'textbook' example is that for λ 550 nm in July. Here, the close similarity of the 2.5 and 5 cm curves indicates these to be nearly unsmoothed records of the shadow pattern; the dominant scale apparently is the Fresnel-zone size, not that of the telescope. At larger apertures, the geometrical aperture dominates; for both 550 and 700 nm, the anticorrelation dip is at nearly twice the delay for 10 cm as for the 5 cm aperture. Thus, the transition between the wave- and the geometrical-optics regimes seems to lie around 5 cm. Such a Fresnel-zone size ( $\simeq \sqrt{\lambda h}$) implies distances to relevant regions of turbulence on the order of 10 km.

The scintillation amplitudes change with aperture size until $\varnothing \lesssim 5$ cm, again indicating the scale when the structures in the 'flying shadows' become resolved: the fluctuation amplitudes then become largely independent of aperture size. On these small spatial scales, also differences in amplitude between different colors become apparent: $\sigma_I^2$ is significantly greater at shorter wavelengths (cf. Paper II).

The variances in summer (July) are significantly and systematically lower than in winter (November), although this is perhaps not striking on the logarithmic scale of the plots.

### 11.6 Power Spectra

The power spectra in Fig. 16 were obtained as direct transforms of the autocovariances in Fig. 15, thus yielding a number of *discrete* data points (as described in Sec. 6). Slightly different sampling times used in summer and winter explains the somewhat different frequency coverage.

With increasing aperture size, the power rapidly decreases

(especially at high frequencies, i.e., scintillation becomes 'slower'), reflecting the spatial averaging of small-scale elements in the shadow pattern. At frequencies $f \gtrsim 100$ Hz, the power density decreases approximately as $f^{-5}$. If the power spectra had been measured to *very* low frequencies, one might have started to see a $1/f$ noise component, often characteristic for atmospheric *transparency* fluctuations (cf. Sec. 6.7.3). We would not expect such a signal to dominate, however, except for quite large apertures ($\gtrsim 1$ m), where scintillation is well averaged out. Aperture effects will be further discussed in Paper III.

### 11.7 Seasonal Differences

At any one site, there can be seasonal variations in scintillation (Diamant et al. 1969; Mikesell 1955; Protheroe 1955a). Power spectra differ primarily at high frequencies, probably due to seasonal changes in jet-stream patterns.

As commented on already, the most striking seasonal effects seen on La Palma are significantly lower $\sigma_I^2$ values in summer, accompanied by more 'textbook'-like autocovariance functions displaying distinct anticorrelation dips. Further, there is some indication that the aperture size, below which $\sigma_I^2$ becomes essentially constant, is somewhat smaller ($\simeq 5$ cm) in summer than in winter ($\simeq 10$ cm). This difference, however, might be an artifact of the different average zenith distances for observation.

### 11.8 Other Dependences

Having completed this first survey of the major functional dependences of atmospheric scintillation, we will next discuss the somewhat subtler dependence on optical wavelength in Paper II. Paper III will be devoted to understanding how scintillation properties are perceived in various types of astronomical telescopes (of different sizes, with or without obscuring secondary mirrors), also evaluating methods to decrease [unwanted] scintillation through apodization of the entrance apertures, or by the application of second-order adaptive optics.

This study is part of the high-speed astrophysics program at Lund Observatory, supported by NFR, the Swedish Natural Science Research Council. The QVANTOS instrument development was supported also by FRN, the Swedish Council for Planning and Coordination of Research. At Lund Observatory, we thank in particular research engineers H. O. Hagerbo, B. Nilsson, and T. Wiesel for their highly competent work on various electronic units. The observations were made at The Research Station for Astrophysics on La Palma (Royal Swedish Academy of Sciences), which is part of the Observatorio del Roque de Los Muchachos of the Instituto de Astrofisica de Canarias. Their staff is thanked for valuable help during our several visits there. Seeing data from the Carlsberg Meridian Circle on La Palma were kindly provided by C. Thoburn of the Royal Greenwich Observatory. V. Dovheden at Lund Observatory performed many of the computations of the higher-order statistical moments. Parts of the material for this paper were prepared by D. Dravins during a visitorship stay at European Southern Observatory in Garching.

## APPENDIX: ACCURACY LIMITS AND ERROR SOURCES

The uncertainties in determined scintillation properties relate to (a) practical limitations due to nonideal instrumentation, and (b) the more fundamental indeterminacy of the nonstationary atmosphere. The latter was discussed in Sec. 5, while here we comment on instrumental limitations. Quite a number of test measurements (in the laboratory, and at the telescope) were made to identify potential sources of inaccuracy, and methods for avoiding them.

### A.1 External Noise Sources?

Our observational procedures were outlined in Sec. 2. Activities such as dome rotation or moving the telescope involve electric transients, which can induce spurious signals in the electronics. Although all detectors and their signal cables were carefully shielded and grounded, the difficulty of finding any true electric ground in the dry volcanic soil at the summit of La Palma called for caution in operating any high-power devices. Therefore, no dome motion, nor telescope re-pointing was ever activated during data recording.

Searches for conceivable external noise signals were made during many hours. Dark-count properties were measured with the detector covered inside a closed dome, while 'bright-count' tests exposed the detector to star-free portions of the sky. However, studies of the statistics of these signals did not suggest the presence of any significant external transients.

### A.2 Dark- and Background Signals

Our measurements were of very bright stars, almost always giving a signal very much higher (by factors $10^3$–$10^4$) than the dark count, or that of the sky background. Therefore, no correction for [the statistics of] the dark nor background counts was made. Such a possible correction would in any case have been quite uncertain.

The dark-count level depends upon the detector's history of prior illuminations. The lowest levels ($\simeq 10$ Hz) were observed after keeping a detector in darkness for several hours, with its high voltage on. A more common level was $\simeq 40$ Hz, rising to above $\gtrsim 100$ Hz following occasional stronger illuminations.

The detectors had passive thermal insulation. As expected, the gradual cooling during a night causes a slight decrease of sensitivity at longer wavelengths (600 and 700 nm), on a level of $\simeq 5\%$. However, such drifts should not affect our results, and nor should the slight differences in color response between different detectors.

In order to collect "all" starlight onto the detector, the focal-plane aperture projected onto the sky was kept quite large ($\simeq 1$ arcmin). The *sky background* (near zenith, with a full Moon low in the sky) generated a count rate of typically $\simeq 100$ Hz through the broadband color filters normally used.

### A.3 Detector Properties

Nonideal behavior of the photomultipliers is our main instrumental concern. Although the detectors had been selected to have the lowest possible afterpulsing, some is still remaining, and does appear to limit some potential studies, given the measuring precision otherwise realized. Likewise, while the nanosecond time scales throughout the electronics do indeed minimize effects of pulse pile-up and dead-times, these effects sometimes become visible at high count rates.

Previous studies have been made of such afterpulsing and dead-time effects (e.g., Foord et al. 1969 [but see comments by Young 1971b]; Gadsen 1965; Gulari and Chu 1978; Saleh 1978; Young 1974), which may influence the details in measured statistical distributions (e.g., Apanasovich and Paltsev 1995; Campbell 1992; Jakeman and Pusey 1980; Selloni 1980; Strohbehn et al. 1975).

### A.4 Variance from Probability Distributions

Tests were made in computing the intensity variance $\sigma_I^2$ from probability distributions measured under various conditions. Different neutral-density filters were used to give widely different (factors of $\simeq$100) count rates, and different sample times were used to vary $\langle n \rangle$, the average number of counts per sample time.

The *true* statistical moments of course remain independent of the count rate and the sample time (as long as it is much shorter than the coherence time of the intensity fluctuations). However, analyses of the apparent statistical moments revealed a dependence of $\sigma_I^2$ on the mean count rate, which could be traced to photomultiplier afterpulsing.

An 'ordinary' sample time produced a 'full' probability distribution histogram with $\langle n \rangle \simeq 10$ (such as in Fig. 2), while a very short sample time gave only an exponential-looking tail with $\langle n \rangle \simeq 1$. The variance was found to be systematically higher in the latter case, especially at low count rates. Laboratory experiments (with both stabilized and modulated light sources) and subsequent calculations confirmed afterpulsing as the cause. For a small $\langle n \rangle$, the deduced variance (and higher moments) is sensitive to the small signal in the tail of the distribution, which is where pairs of pulses occurring within one sample time are recorded.

The conclusion is that a suitably high $\langle n \rangle$ yields more reliable results, and that differential measurements should be made with the same $\langle n \rangle$. The count rate itself, as long as it is reasonable, does not affect the estimate of sigma. Therefore, whenever possible, the sampling time was adjusted to give $\langle n \rangle$ in the range of 5–10. For differential measurements, an attempt was made to set the precise sample time such, that $\langle n \rangle$ would agree to within two decimal places, an adjustment whose accuracy was sometimes limited by changes in the atmosphere itself.

### A.5 Variance from Autocorrelations

As described in Sec. 6, $\sigma_I^2$ was also determined from autocorrelations. The parameter limits for their accurate measurement were explored. For example, neutral filters of densities 0, 1, 2, and 3 were used, correspondingly increasing the sample times from 1 $\mu$s, 10 $\mu$s, 100 $\mu$s, to 1 ms, but keeping $\langle n \rangle$ very small ($\simeq$1). Despite this, there really was no significant difference in the measured variance. Only when provoking very high count rates ($\simeq$1 MHz), or extremely long sample times ($\simeq$10 ms, comparable to the time scale of scintillation itself), did systematic differences appear.

The conclusion is that the variance, as determined from autocorrelations, does *not* seem to be significantly affected by reasonable choices of observational parameters, in contrast to that determined from probability distributions which, for unfortunate parameter combinations, can become quite sensitive to afterpulsing.

### A.6 Autocorrelations

The stability of the measured autocorrelation shapes was examined in various ways. To examine any possible dependence on different data handling in the signal processor, e.g., for different clip levels, a range of neutral density filters was used to 'provoke' poor data quality, combined with clip levels chosen far off the normal values. Even double-clipped functions (i.e., binary clipping of *both* multiplicative factors producing the autocorrelation function) were tried, as well as various levels of 'scaling' (decrease of the signal amplitude by only recording every $n$th photon count; see Saleh (1978) for descriptions of such data treatment methods). Despite all these actions, the computed autocorrelation functions (after normalization to 1) appear surprisingly stable, and (except for the increased noise in some cases) retain their shape, halfwidths, etc.

A possible detector dependence was examined by alternate measurements with two different photomultipliers. However, when normalized to unity, there were no significant differences.

The conclusion is that changing observational parameters (within reasonable limits) has only an insignificant effect on resulting autocorrelation functions.

### A.7 Auto- Versus Cross Correlation

The discussion so far refers to autocorrelation functions on the dominant scintillation time scales, i.e., *milli*seconds. A somewhat different situation occurs on *micro*second time scales, where the atmospheric signal is small, and extensive averaging is required to bring it out. Then, afterpulsing effects on such time scales may become visible. The need for a large signal invites high count rates, causing also dead-time and pulse-pile-up effects to enter.

In measured autocorrelations there is clearly visible an [afterpulsing] rise for delays $\lesssim$1 $\mu$s, and a [dead-time] decrease for the very shortest time lags ($\lesssim$60 ns). To circumvent these effects, the studies made for the shortest time scales are not *auto*correlations, but rather *cross* correlations between two different detectors, placed after a beamsplitter. For any one photon count, the probability of afterpulsing is low, and the remaining afterpulsing signal in cross correlation decreases as the *square* of this already low probability; no significant afterpulsing is visible in actual data. This increased accuracy carries a penalty in photometric precision:

the signal is halved by the beamsplitter, so the correlation product decreases a factor 4.

On *extremely short* time scales, otherwise not discussed in this paper ($\lesssim$100 ns), there actually is a noticeable increase also of the measured cross correlation, probably due to afterpulsing which, after all, has some statistical similarities between two detectors of similar construction. Correlated signals could also come from cosmic-ray showers where particles hit both detectors almost simultaneously. Also, at these very shortest time scales, an increased correlation due to the quantum-mechanical bunching of photons in thermal light will ultimately become visible.

### A.8 Limitations to Probability Distributions

In our measurements of auto- and cross correlation, and autocovariance functions, the [by far] dominant source of inaccuracy is the nonstationarity of the atmosphere (combined with the nonsimultaneity of different measurements); *not* detector nor other instrumental effects. However, the measurement of probability distribution functions, and in particular the accurate determination of their higher statistical moments, may be affected by detector properties. On La Palma, we recorded many hundreds of such functions (for the dependence on telescope aperture size, zenith distance, etc.). Although, quite possibly, data of better quality are not available elsewhere, we have refrained from presenting them here because of the difficulty of understanding which significant digit various subtle detector effects may enter. Some of these effects depend on both the instantaneous detector illumination and on its past history, in practice precluding laboratory calibrations. Therefore, the discussion in Sec. 5 should perhaps be seen as a pilot study for exploring the limits to statistical determinations, possibly to be revised as more perfect detectors become available.

## REFERENCES


Agabi, A., Borgnino, J., Martin, F., Tokovinin, A., and Ziad, A. 1995, A&AS, 109, 557

Akimov, L. A., Belkina, I. L. Dyatel, N. P., and Marchenko, G. P. 1992, Kin. Phys. Celest. Bodies, 8, No. 3, 57 (Kin. Fiz. Nebesnykh Tel 8, No. 3, 63)

Aleksandrov, A. P., et al. 1990, Izv. Atmos. Oceanic Phys., 26, 1 (Izv. Akad. Nauk SSSR, Fiz. Atmos. Okeana, 26, 5)

Alexeeva, G. A., and Kamionko, L. A. 1982, Izv. Glavn. Astron. Obs. (Pulkovo), No. 200, 63

Andrews, L. C., and Phillips, R. L. 1985, JOSA A, 2, 160

Apanasovich, V. V., and Paltsev, S. V. 1995, JOSA B, 12, 1550

Ardeberg, A. 1984, in Site Testing for Future Large Telescopes, ESO Conf. Proc. 18, ed. A. Ardeberg and L. Woltjer, p. 73

Azouit, M., Vernin, J., Barletti, R., Ceppatelli, G., Righini, A., and Speroni, N. 1980, J. Appl. Meteorol., 19, 834

Barakat, R. 1976, JOSA, 66, 211

Barletti, R., Ceppatelli, G., Paternò, L., Righini, A., and Speroni, N. 1976, JOSA, 66, 1380

Barletti, R., Ceppatelli, G., Paternò, L., Righini, A., and Speroni, N. 1977, A&A, 54, 649

Beckers, J. M. 1993, Sol. Phys., 145, 399

Ben-Yosef, N., and Goldner, E. 1988, Appl. Opt., 27, 2167

Beran, M. J., and Whitman, A. L 1988, Appl. Opt., 27, 2178

Bester, M., Danchi, W. C., Degiacomi, C. G., Greenhill, L. J., and Townes, C. H. 1992, ApJ, 392, 357

Briggs, J. 1963, Meteorol. Mag., 92, 69

Bufton, J. L. 1973, Appl. Opt., 12, 1785

Bufton, J., and Genatt, S. H. 1971, AJ, 76, 378

Burnashev, V. I., Burnasheva, B. A., Merkulova, N. I., and Metik, L. P. 1991, Bull. Crimean Astrophys. Obs., 83, 140 (Izv. Krymskoi Astrofiz. Obs. 83, 156)

Buscher, D. F., et al. 1995, Appl. Opt., 34, 1081

Butler, H. E. 1952, Proc. Roy. Irish Acad., 54A, 321 (Contrib. Dunsink Obs. (Dublin), No. 4, 1)

Caccia, J. L., Azouit, M., and Vernin, J. 1987, Appl. Opt., 26, 1288; erratum *ibid.* 26, 3185

Campbell, L. 1992, Rev. Sci. Instrum., 63, 5794

Campbell, L., and Elford, W. G. 1990, J. Atmos. Terr. Phys., 52, 313

Clarke, D. 1980, MNRAS, 190, 641

Clifford, S. F. 1978, in Laser Beam Propagation in the Atmosphere, ed. J. W. Strohbehn (Berlin, Springer), p. 9

Colavita, M. M., Shao, M., and Staelin, D. H. 1987, Appl. Opt., 26, 4106

Consortini, A. 1991, in International Trends in Optics, ed. J. W. Goodman (San Diego, Academic), p. 267

Cook, M. C. 1991, J. Mod. Opt., 38, 821

Coulman, C. E., and Vernin, J. 1991, Appl. Opt., 30, 118

Coulman, C. E., Vernin, J., Coqueugniot, Y., and Caccia, J. L. 1988, Appl. Opt., 27, 155

Coulman, C. E., Vernin, J., and Fuchs, A. 1995, Appl. Opt., 34, 5461

Cummins H. Z., and Pike, E. R. (eds.) 1974, Photon Correlation and Light Beating Spectroscopy (New York, Plenum)

Dainty, J. C., Levine, B. M., Brames, B. J., and O'Donnell, K. A. 1982, Appl. Opt., 21, 1196

Dalaudier, F., Sidi, C., Crochet, M., and Vernin, J. 1994, J. Atmos. Sci., 51, 237

Darchiya, Sh. P. 1966, in Optical Instability of the Earth's Atmosphere, ed. N. I. Kucherov (Jerusalem, Israel Program for Scientific Translations), p. 82

Davis, J., Lawson, P. R., Booth, A. J., Tango, W. J., and Thorvaldson, E. D. 1995, MNRAS, 273, L53

de Vos, M. 1993, Ph.D. thesis, University of Groningen

Deubner, F. L., and Isserstedt, J. 1983, A&A, 126, 216

Diamant, E. M., Kolchinsky, I. G., and Filippov, Yu. K. 1969, Astrometr. Astrofiz. (Kiev), 5, 100

Dravins, D. 1994, ESO Messenger, No. 78, 9

Dravins, D., Hagerbo, H. O., Lindegren, L., Mezey, E., and Nilsson, B. 1994, in Instrumentation in Astronomy VIII, ed. D. L. Crawford and E. R. Craine, Proc. SPIE 2198, 289

Dravins, D., Lindegren, L., Mezey, E., and Young, A. T. 1997a, PASP (submitted) [Paper II]

Dravins, D., Lindegren, L., Mezey, E., and Young, A. T. 997b, PASP, in preparation [Paper III]

Dunlop, C. N., Hamam, Y. A., and Major, J. V. 1989, MNRAS, 236, 875

Ellison, M. A., and Seddon, H. 1952, MNRAS, 112, 73

Elsässer, H. 1960, Die Naturwissenschaften 47, 6 (Mitt. Astron. Inst. Tübingen, Nr. 40)

Filippov, Yu. K. 1972, Astrometr. Astrofiz. (Kiev), 17, 108

Flatté, S. M., Bracher, C., and Wang, G. Y. 1994, JOSA A, 11, 2080

Foord, R., Jones, R., Oliver, C. J., and Pike, E. R. 1969, Appl. Opt., 8, 1975

Frehlich, R. G., and Churnside, J. H. 1989, J. Mod. Opt., 36, 1645

Fried, D. L., Mevers, G. E., and Keister, M. P. 1967, JOSA, 57, 787

Frisch, U. 1995, Turbulence: The Legacy of A. N. Kolmogorov (Cambridge, Cambridge University Press)
Fuentes, F. J., Fuensalida, J. J., and Sanchez-Magro, C. 1987, MNRAS, 226, 769
Fürth, R. 1956, in Astronomical Optics, ed. Z. Kopal (Amsterdam, North-Holland), p. 300
Gadsden, M. 1965, Appl. Opt., 4, 1446
Georgobiani, D., Kuhn, J. R., and Beckers, J. M. 1995, Sol. Phys., 156, 1
Gladyshev, S. A., Dadurkjavichus, V., Ovchinnikov, A. A., Popov, V. V., Pjatrauskas, I., and Ralis, R. 1987, in Metody Povyshenija Effektivnosti Opticheskih Teleskopov, ed. S. A. Gladyshev (Moscow, Sternberg Astron. Inst.), p. 39
Goldner, E., and Ben-Yosef, N. 1988, Appl. Opt., 27, 2172
Grec, G., Fossat, E., Brandt, P., and Deubner, F. L. 1977, A&A, 77, 347
Gulari, E., and Chu, B. 1978, Rev. Sci. Instrum., 48, 1560
Gracheva, M. E., and Gurvich, A. S. 1965, Radiophys. Quantum Electron. (USSR), 8, 511 (Izv. VUZ Radiofizika 8, 717)
Hall, P. 1982, Rates of Convergence in the Central Limit Theorem (London, Pitman)
Hill, R. J. 1992, Waves Random Media, 2, 179
Hill, R. J., and Churnside, J. H. 1988, JOSA A, 5, 445
Høg, E. 1968, Z. Astrophys., 69, 313
Hosfeld, R. 1954, JOSA, 44, 284
Hudson, C. C. 1965, Nature, 207, 247
Ishimaru, A. 1978, Wave Propagation and Scattering in Random Media. Vol. 2: Multiple Scattering, Turbulence, Rough Surfaces, and Remote Sensing (New York, Academic)
Jakeman, E., Parry, G., Pike, E. R., and Pusey, P. N. 1978, Contemp. Phys., 19, 127
Jakeman, E., Pike, E. R., and Pusey, P. N. 1976, Nature, 263, 215
Jakeman, E., and Pusey, P. N. 1980, in Inverse Scattering Problems in Optics, ed. H. P. Baltes (Berlin, Springer), p. 73
Keller, G., Protheroe, W. M., Barnhart, P. E., and Galli, J. 1956, Investigations of Stellar Scintillation and the Behavior of Telescopic Images, Perkins Obs. reprint No. 39 (Ohio State University)
Kendall, M., and Stuart, A. 1977, The Advanced Theory of Statistics, 4th ed., Vol. 1 (High Wycombe, Charles Griffin)
Knoechel, G., and von der Heide, K. 1978, A&A, 67, 209
Kravtsov, Yu. A. 1992, Rep. Prog. Phys., 55, 39
Kravtsov, Yu. A. 1993, Appl. Opt., 32, 2681
Lawrence, R. S., and Strohbehn, J. W. 1970, Proc. IEEE, 58, 1523
Lee, R. W. 1969, Radio Sci., 4, 1211
Lee, R. W., and Harp, J. C. 1969, Proc. IEEE, 57, 375
Lightsey, P. A. 1994, Opt. Eng. (Bellingham), 33, 2535
Lumley, J. L., and Panofsky, H. A., 1964, The Structure of Atmospheric Turbulence (New York, Wiley-Interscience)
Majumdar, A. K. 1984, Opt. Commun., 50, 1
Mariotti, J. M. 1983, Opt. Acta, 30, 831
Martin, J. M., and Flatté, S. M. 1988, Appl. Opt., 27, 2111
Mertz, L. 1965, Transformations in Optics (New York, Wiley), p. 12
Mikesell, A. H. 1955, The Scintillation of Starlight (Washington, D.C.), Publ. U.S. Naval Observatory 2nd Ser., Vol. XVII, part IV, p. 139.
Mikesell, A. H. , and Brown, C. S. 1966, AJ, 71, 393
Mikesell, A. H., Hoag, A. A., and Hall, J. S. 1951, JOSA, 41, 689
Mitchell, R. L. 1968, JOSA, 58, 1267
Morris, G. J. 1971, Phys. Rev. Lett., 27, 1600
Muñoz-Tuñon, C., and Fuentes, F. J. 1990, Ap&SS, 171, 257
Nettelblad, F. 1953, Medd. Lunds Astron. Obs., Ser. II, No. 130
Nightingale, N. S., and Buscher, D. F. 1991, MNRAS, 251, 155
Oosterhoff, P. Th., ed. 1957, Transactions IAU, IX, 345
Panofsky, H. A., and Dutton, J. A. 1984, Atmospheric Turbulence (New York, Wiley-Interscience)
Parry, G., Pusey, P. N., Jakeman, E., and McWhirter, J. G. 1977, Opt. Commun., 22, 195
Parry, G., and Walker, J. G. 1980, JOSA, 70, 1157
Parry, G., Walker, J. G., and Scaddan, R. J. 1979, Opt. Acta, 26, 563
Paternò, L. 1976, A&A, 47, 437
Protheroe, W. M. 1955a, Contrib. Perkins Obs. (University of Ohio), Ser. II, No. 4, p. 28
Protheroe, W. M. 1955b, JOSA, 45, 851
Protheroe, W. M. 1961, Science, 134, 1593
Protheroe, W. M. 1964, Quart. J. Roy. Meteorol. Soc., 90, 27
Redfern, R. M. 1991, Vistas Astron., 34, 201
Reiger, S. H. 1963, AJ, 68, 395
Rocca, A., Roddier, F., and Vernin, J. 1974, JOSA, 64, 1000
Roddier, C., and Vernin, J. 1977, Appl. Opt., 16, 2252
Roddier, F. 1981, Progr. Opt., 19, 281
Rosa, F., and Fuensalida, J. J. 1990, Ap&SS, 171, 283
Rytov, S. M., Kravtsov, Yu. A., and Tatarskii, V. I. 1989, Principles of Statistical Radiophysics 4. Wave Propagation Through Random Media (Berlin, Springer)
Saleh, B. 1978, Photoelectron Statistics (Berlin, Springer)
Sasiela, R. J. 1994, Electromagnetic Wave Propagation in Turbulence, Evaluation and Applications of Mellin Transforms (Berlin, Springer)
Schmidt-Kaler, T., and Winkler, C. 1984, A&A, 136, 299
Selloni, A. 1980, in Inverse Scattering Problems in Optics, ed. H. P. Baltes (Berlin, Springer), p. 117
Seykora, E. J. 1993, Sol. Phys., 145, 389
Siedentopf, H., and Elsässer, H. 1954, Z. Astrophys., 35, 21 (Mitt. Astron. Inst. Tübingen, Nr. 14)
Stecklum, B. 1985, Astron Nachr., 306, 145
Stock, J., and Keller, G. 1960, in Telescopes, ed. G. P. Kuiper and B. M. Middlehurst (Chicago, University of Chicago Press), p. 138
Strohbehn, J. W. 1978, in Laser Beam Propagation in the Atmosphere, ed. J. W. Strohbehn (Berlin, Springer), p. 45
Strohbehn, J. W., Wang, T. I., and Speck, J. P. 1975, Radio Sci., 10, 59
Stroud, P. 1996, Opt. Eng. (Bellingham), 35, 543
Stull, R. B. 1988, An Introduction to Boundary Layer Meteorology (Dordrecht, Kluwer)
Tatarski, V. I. 1961, Wave Propagation in a Turbulent Medium (New York, McGraw-Hill); reprint 1967 (New York, Dover)
Tatarskii, V. I. 1971, The Effects of the Turbulent Atmosphere on Wave Propagation (Jerusalem, Israel Program for Scientific Translations)
Tur, M. 1985, JOSA A, 2, 2161
Uscinski, B. J. 1977, The Elements of Wave Propagation in Random Media (New York, McGraw-Hill)
Uscinski, B. J. 1985, JOSA A, 2, 2077
Vernin, J., and Azouit, M. 1983, J. Optics, 14, 131
Vernin, J., Barletti, R., Ceppatelli, G., Paternò, L., Righini, A., and Speroni, N. 1979, Appl. Opt., 18, 243
Vernin, J., and Muñoz-Tuñón, C. 1992, A&A, 257, 811
Vernin, J., and Muñoz-Tuñón, C. 1994, A&A, 284, 311
Vernin, J., and Roddier, F. 1973, JOSA, 63, 270
Vid'machenko, A. P. 1994, Kin. Phys. Celestial Bodies 10, No. 5, 52 (Kin. Fiz. Nebesnykh Tel 10, No. 5, 62)
Warner, B. 1988, High-Speed Astronomical Photometry (Cambridge, Cambridge University Press)
Wessely, H. W., and Mitchell, M. P. 1971, JOSA, 61, 242
Young, A. T. 1967, AJ, 72, 747
Young, A. T. 1969, Appl. Opt., 8, 869

Young, A. T. 1970a, JOSA, 60, 248
Young, A. T. 1970b, JOSA, 60, 1495
Young, A. T. 1971a, Sky and Telescope, 42, 139
Young, A. T. 1971b, Appl. Opt., 10, 1681
Young, A. T. 1974, in Methods of Experimental Physics, Vol. 12, Astrophysics, part A: Optical and Infrared, ed. N. Carleton (New York, Academic), p. 1
Zhukova, L. N. 1958, Izv. Glavn. Astron. Obs. (Pulkova) 21, No. 162, 72
Zwicky, F. 1950, PASP, 62, 150